

## Foreword

During the time when we were actively considering a liquid scintillator detector for MINOS, we received a lot of help from several Mechanical Engineering graduate students working under the direction of Professor Tom Chase of the University of Minnesota ME Department. In particular, Matt Hansen did a lot of mechanical design and testing involving the mechanical properties of PVC cells containing Bicron 517L liquid scintillator.

**This NOvA note consists of the final chapters of Matt Hansen's Masters thesis, which was entitled "The Design and Testing of a Liquid Scintillator High Energy Particle Detector", January 1999.** It describes the results of many of the mechanical tests that were carried out, all of which are relevant to our NOvA design. They involve creep tests, seal testing, effects of scintillator on mechanical constants, etc. Chapter 4 is the most relevant to NOvA but at the end of chapter 3 there are some comments on in-situ repair techniques, in case the PVC extrusions are (slightly) damaged during construction.

These tests were done with commercial 8-cell extrusions from L.B.Plastics which were nominally 1 inch x 8 inch. The outer walls were 1.5 mm thick (+- 20% in places) with inner web about half that, although that thickness was highly variable. The inner cell sizes were close to 2 cm x 2 cm.

While these mechanical tests were being carried out, we were also measuring light yields from many different scintillators in PVC and other plastics, using heated samples to accelerate aging, looking for effects of aging, interactions on WLS fibers, etc. The results of all the relevant tests are described in a NIM article that we wrote, and that not everyone in the collaboration seems to be aware of:

P. Border et al., NIM A463 (2001), p 194-204

In addition, I also presented some relevant data at the first Off-Axis Workshop, which was held at SLAC. That can be found by following one's nose from the NOvA web page.

Keith Ruddick

# Chapter 3

## Manufacturing Plan

The manufacture of the liquid scintillator active detector consists of two main parts. The assembly plan is addressed in section 3.1. The quality assurance plan is discussed in section 3.2. The manufacture of individual parts used in the detector is beyond the scope of this document and will not be discussed. For a detailed description of individual parts reference chapter 2.

### 3.1 Assembly Plan

The following section contains a description of the assembly plan for the active detector design. The first step of the assembly process is the fiber preparation. The next step is the assembly of the modules. Certain portions of the module assembly can be performed in parallel with the fiber preparation. After the modules are assembled, the modules are shipped to the mine, where all parts are installed into the detector. Figures 3.1 and 3.2 are flowcharts of the manufacturing process that shows the major tasks during the assembly of an active detector plane. The position of the quality control checkpoints will only be noted in this section. For a complete discussion of quality control methods, please reference section 3.2.

#### 3.1.1 Fiber Preparation

Fiber preparation is a critical path during detector construction. The fibers are fragile and must be handled carefully to prevent damage.

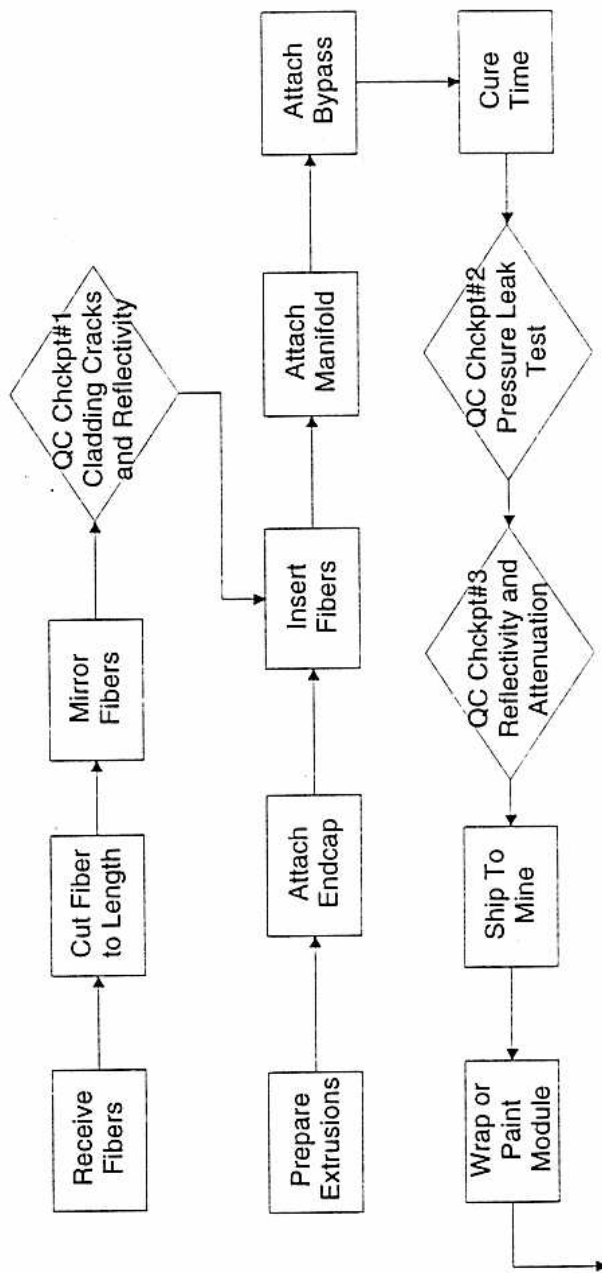


Figure 3.1: Flowchart Showing the Major Manufacturing Operations

After receiving the fibers from a manufacturer, the fibers are cut to the necessary lengths. Five different fiber lengths correspond to the five different extrusion lengths. The fiber length is approximately one-half meter longer than the extrusion module. The extra length is required for routing the fiber through the manifold. This extra length also permits the fiber to be re-mirrored if the reflectivity is inadequate. After the manifold is attached to the module, any extra fiber extending from the module is removed and discarded.

After the fibers are cut to length, a mirror is applied to one end of the fiber. The mirror is necessary because only a few photons of energy are captured during an event. At the point where light enters the fiber, 50% of the photons travel in one direction, while the remaining 50% travel in the other. For example, if 6 photons are captured by the fiber, then 3 photons travel to the photomultiplier tube (PMT), while 3 travel away from the PMT. The 3 photons that travel away from the PMT are lost if there is no mirror. With extremely low light levels, it is possible for the PMT to lose a small signal in the noise and miss an event. With a mirrored end, the PMT will sense a 6 photon peak, a level that will not be filtered out.

Fermilab has developed a process for polishing and mirroring large numbers of fibers. First, the fibers are bundled into groups of 50. Next, fiber bundles are dipped into liquid nitrogen. The frozen end of the bundle is then machined with a flycutter. The first pass rough cuts the bundle. The second pass, which removes about 0.003 cm (0.001 in) of material, polishes the fiber ends. The polished end is suitable for sputtering.

Sputtering is essentially the vaporization of a material within a vacuum. The end of the fiber bundle is placed within a vacuum chamber. The chamber also contains a small sample of aluminum. A large electric current is passed through the aluminum. The heat caused by the resistance of the aluminum to the current causes the metal to vaporize. The aluminum vapor is deposited on all other surfaces within the vacuum chamber, including the fiber ends. After sputtering, the end of each fiber is covered with a quick-curing epoxy, which protects the mirrored surface.

The fibers undergo a quality assurance test before installation into the module. This quality assurance test checks two different fiber qualities. The first test scans the surface of the fiber for cracks or defects. The second test measures the reflectivity of the mirror. Fibers that pass both quality tests are ready for use in the extrusions.

### 3.1.2 Module Assembly

The module assembly consists of three major segments. The first segment is extrusion preparation. Some portions of the extrusion preparation can be performed in parallel with fiber preparation. The second part is endcap installation. The third segment is the bypass installation. The module assembly is the most time consuming and labor intensive step of the manufacturing process.

#### 3.1.2.1 Extrusion Preparation

Extrusion preparation is the first step in the manufacturing of an active detector plane. The extrusions are unpacked and then cut to length. A laborer then moves the extrusions to a preparation table where the extrusions are prepared for the installation of the endcaps and bypass. Figure 3.3 is a flowchart that details the module preparation.

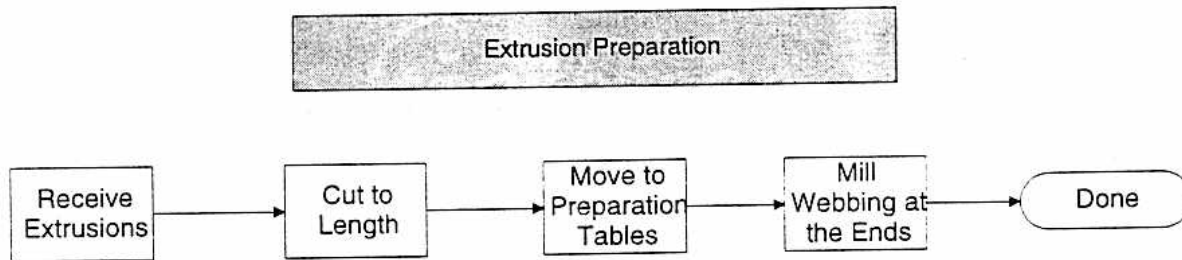


Figure 3.3: Flowchart Detailing Extrusion Preparation

After the factory receives the extrusions from the manufacturer, an operator unpacks the extrusions and clamps the extrusion in a fixture. The fixture holds the extrusion while the operator cuts the extrusion to the proper length. The manufacturer supplies the extrusions in the longest length required, 792 cm (312 in). The operator only needs to cut the extrusions that require 45° ends. The ends on the as manufactured extrusions are acceptable for use and do not require "dressing". The operator uses a common radial arm saw to cut the extrusions. The operator must produce 4 different extrusion lengths. The extrusions are then loaded onto carts and moved to the preparation tables.

The extrusions are prepared for the endcaps at the preparation tables. The operator uses a machining head to remove the first 1.27 cm (0.50 in) of the inner web from the extrusion. Using a custom ground end mill will increase the efficiency of this step. This material is removed so the endcap may fit. The operator must fixture the extrusion for this step. After the laborer finishes this operation, the extrusion is ready for the installation of the endcaps.

### 3.1.2.2 Endcap Installation

The endcap installation is the final assembly operation performed before shipment to the mine for modules not requiring a bypass. This step contains two different assembly operations. The first operation is the lower endcap installation and fiber insertion. The second operation is the manifold, or upper endcap, installation. These operations are serial tasks. Reference figures 3.1 and 3.2 for the placement of these tasks in the overall assembly process.

**3.1.2.2.1 Lower Endcap Installation and Fiber Insertion** PVC cement holds the lower endcap in place. An operator applies a primer to the mating surfaces of the endcap, as well as the extrusion. Next, the operator applies the epoxy to the necessary surfaces of the endcap. The endcap is now ready for insertion into the extrusion. The operator slides the endcap into position by hand. It is not necessary to use a machine for this step. A simple jig or clamp holds the endcap in place while the epoxy cures. Minimal holding force is required during the curing process.

The fibers are inserted into the extrusion after the lower endcap is in place, as explained in Berg (1997).

**3.1.2.2.2 Manifold Installation** Attaching the manifold is one of the most complex and critical processes of the module assembly. As discussed in section 2.4, the order of the fibers must be preserved between the extrusion and optical connector. The manifold must also mate with the extrusion with an air-tight seal. Any leaks will allow the scintillator vapors to escape to the mine enclosure and produce a possible health hazard. Figure 3.4 is a flowchart that details the installation of the manifold.

The routing tray is the first component of the manifold installed. An operator places

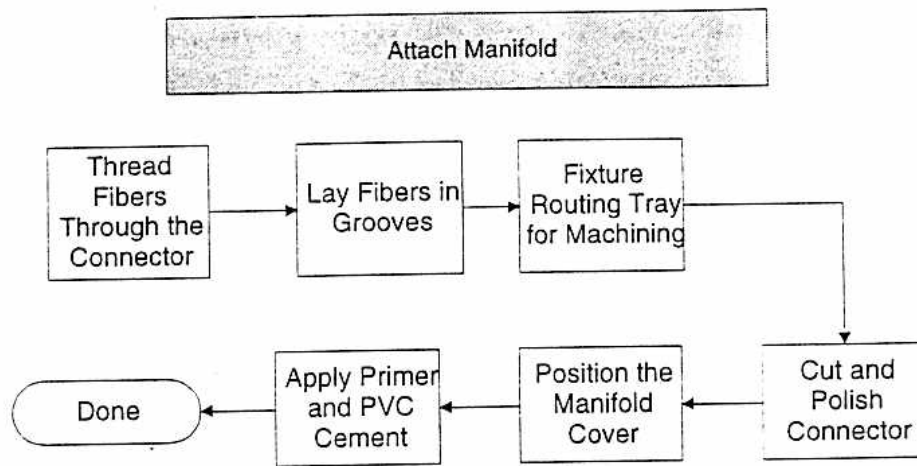


Figure 3.4: Flowchart Detailing the Installation of the Manifold

the tray flush to the open end of the extrusion. Next, the operator snaps the fibers into grooves on the tray. The operator must use care and caution during this step both to prevent damage to the fibers, as well as to insure correct placement of the fibers. After the fibers are in the grooves, the laborer gathers the free ends and pushes the ends through the holes in the optical connector.

The manifold cover attaches to the extrusion in a similar manner as the lower endcap except for the handling of the fibers. After the fibers are fed through an opening in the far end of the manifold cover, the operator slides the cover partly over the routing tray. Before the cover is slid completely into place, the laborer applies the primer and epoxy to the cover just as for the lower endcap. A fixture similar to the jig used on the lower endcap holds the manifold in place while the epoxy cures. Figure 2.10 on page 23 is a drawing that shows how the routing tray nests inside of the manifold. Note that the optical connector is not shown in the figure.

The installation of the optical connector, which is the last step in the assembly of the manifold, is a simple, but important assembly procedure. The connector must mate with the manifold cover with a leak-proof seal, or the module will fail the pressure tests.

After the fibers placed in the connector, a technician seals the manifold. Five-minute

epoxy is injected into the connector. This epoxy has a dual purpose. The epoxy holds the fibers rigidly in place to produce a proper optical connection, and also produces an airtight seal around the fibers. The technician also applies epoxy around the cracks around the connector to finish the seal.

The polishing process for the connector is similar to the polishing of the fibers during the mirroring process. A couple of differences between this process and the mirroring method exist though. The connector is not dipped into liquid nitrogen prior to machining. Only one connector is prepared at a time, unlike the fibers, where many are polished at once. The flycutting process is the same as in fiber mirroring. Refer back to section 3.1.1 for a description of the fiber mirroring process.

### 3.1.2.3 Bypass Installation

Modules requiring a bypass are assembled on a different preparation table than modules that do not require a bypass. This arrangement reduces the equipment requirements for the assembly process. For a layout of the assembly area see Berg (1997). Figure 3.5 is a flowchart that details the installation of the bypass.

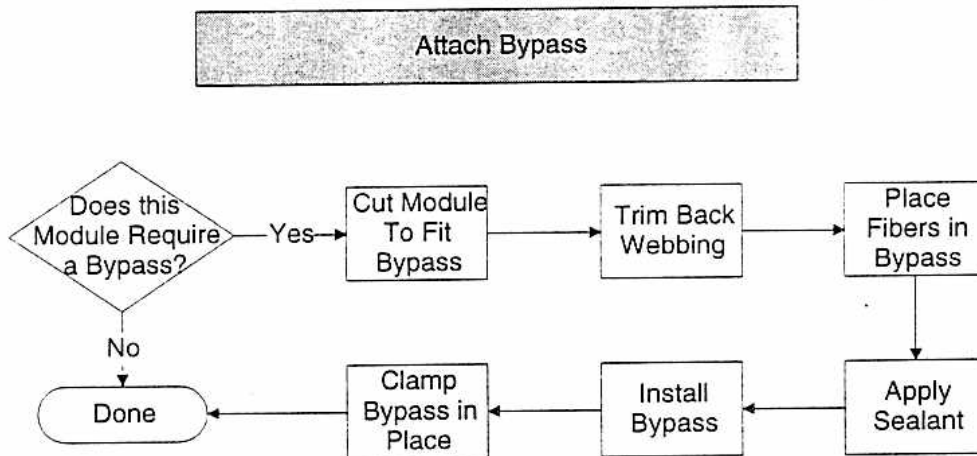


Figure 3.5: Flowchart Detailing the Bypass Installation

The semi-circular hole that accommodates the bypass is created in two steps. First, the operator cuts out the hole using a jig saw on a swing arm. Next, the jig saw

is removed and a router is installed on the swing arm. The router cuts back the internal web of the extrusion. This step must be performed before inserting the fibers, otherwise the fibers will be destroyed. Refer to section 2.3 on page 18 for a description of the seal design.

The bypass seal design is robust and accommodates large tolerances. Consequently, cutting the extrusion does not require a high precision machine like a CNC mill. This operation does require many different operations from the technician, so it may be possible that an inexpensive portable mill could lower operational expenses. The author has not developed a detailed cost analysis to recommend which process is better.

The operator must use care when inserting the fibers into the bypass. The insertion is performed before the bypass is fully installed. To do this task, the operator must pull the fiber partially out of the extrusion and lay the fiber into the grooves in the bypass. The operator then slides the bypass into place and snaps the ends under the extrusion's outside edge. The operator must make sure the fibers still reach the end of the extrusion after the bypass is in place.

Sealing the bypass is an almost identical operation to sealing the manifold and lower endcap. Primer is applied to both the bypass and extrusion, while the PVC cement is only applied to the bypass. Because the end of the bypass snaps into place, the operator should apply some cement to the outside of the snap fit to insure a proper seal in this location. The bypass should be insulated from shock loads until the epoxy has cured.

### 3.1.3 Mine Assembly

This section describes the manufacturing operations that occur at the mine. All previously described operations can occur at a specially prepared mine factory, but it is assumed the majority of the assembly process will occur at research institutions. The majority of this section describes the steps performed to prepare the steel planes for mounting the plastic extrusions. Lawrence Livermore National Lab is responsible for the steel manufacturing plan<sup>1</sup>, and consequently the manufacture of steel planes is not discussed in this document. Figures 3.1 and 3.2 illustrate where the following

---

<sup>1</sup>Subsequently, the steel responsibility has been transferred to Fermilab.

operations are located in relation to the other manufacturing operations.

After the modules are received at the mine, the modules are wrapped in black plastic to produce a light barrier. The white PVC used for the modules is not light tight, so light in the mine can enter the fibers and increase the background noise. The modules are light-leak and reflectivity tested after this operation.

Before the modules are mounted, several parts are attached to the steel plane. The band brackets and gutters are welded into place while the steel plane is still on the strong-back. Also, studs used to support the modules are welded into place using a stud gun. The studs are placed every 18.9 cm (7.4 in) on the four edges of the plane used to support the modules. Every sixth plane has PMT stands and cable trays attached. These components must also be welded to the steel before mounting modules.

The band brackets are aligned to the steel using crude surveying techniques. A line connecting two corners on the steel plane is the base line. This line should be oriented at a 45° to horizontal once the steel plane is installed into the detector. Next, a line traveling through the center of the magnet hole and perpendicular to the baseline is created. This centerline line sets the lateral position for the brackets. Subsequent layout lines are created parallel yet offset to the centerline. Bracket location is determined by measuring from the baseline along the parallel lines.

The steel plane is now ready for the modules. Operators lay the modules in place and use metal bands to fix the modules to the steel. The bands, which have a 1.27 cm (0.5 in) by 0.038 cm (0.015 in) cross section, are crimped into loops by a hand held tool. After the modules are in place, the modules are pressure tested again to make sure the banding and shipping processes did not cause leaks. After the plane is hung, technicians will connect the modules to the PMTs. This last step completes the assembly process for a single plane of the detector.

### 3.2 Quality Assurance Plan

This section describes the quality assurance plan and the maintenance plan for the active detector. The plan includes 6 different quality control checkpoints. The first, third and fifth checkpoints all measure the reflectivity and attenuation of the fibers used in a module. The first checkpoint also inspects for cracks in the outer cladding

of the fiber. The second and sixth checkpoints pressure test the modules for air leaks. The fourth checkpoint inspects the light barrier for light leaks. Methods to repair the modules are explained at the end of this section.

The quality assurance plan described in this document is comprehensive. It may be possible to eliminate some of the tests performed after a confidence in the process is developed. For example, during the design stages of this project two planes worth of fiber was checked for cracks, and no cracks were found. It is probable that this test is unnecessary and can be eliminated from the manufacturing process at some later date.

### 3.2.1 Cladding Cracks and Mirror Reflectivity

This section describes quality assurance tests that evaluate fiber fitness. Two tests determine the quality of a fiber. One test checks for cracks in the outer cladding of the fiber. The other test measures the reflectivity of the mirror on the end of the fiber.

The first quality assurance checkpoint evaluates the fiber cladding and mirror reflectivity, while the third and sixth checkpoints only measure reflectivity. Figure 3.6 is a flowchart that details the process for checkpoint number 1. Figure 3.7 is shown to compare and contrast the first checkpoint to the third and fifth checkpoints. Figures 3.1 and 3.2 illustrates where these quality assurance tests are included in the overall manufacturing process.

#### 3.2.1.1 Cladding Cracks

The fibers are tested for cracks in the cladding for two main reasons. First, cracks can lower the amount of light collected by the PMTs. Second, the fiber core dissolves in liquid scintillator and cracks can expose the core to the scintillator. This check may occur while the fiber is still on the spool or after the the operator cuts the fiber to length.

Cladding cracks are small defects on the surface of the fiber. The crack is problematic only when it extends to the fiber core. The light captured by the fiber travels through the core of the fiber. The difference in the index of refraction of the cladding and core keep the light in the fiber. Cracks that extend to the core allow light to escape

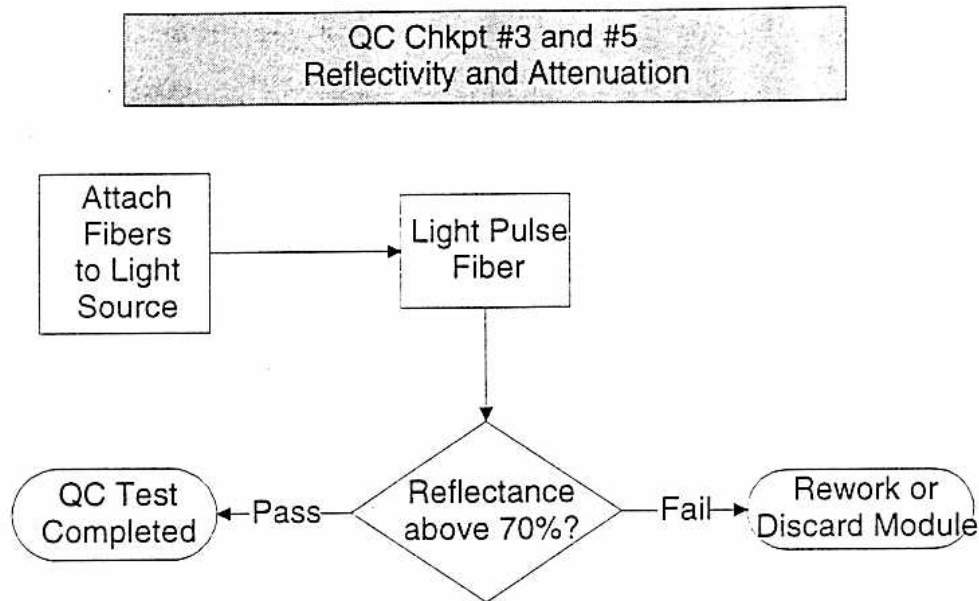


Figure 3.7: Flowchart Detailing the Third and Fifth Quality Control Checkpoints

from the fiber.

A simple machine automates the inspection process. The machine contains unwind and rewind stands, as well as a light source, light meter and cut off stand.

The operator loads the fiber spool onto an unwind stand and threads the end of the fiber through the light source and the meter. After the light meter, the fiber strand passes through neoprene-coated pinch rollers and onto a rack.

The light source is a simple bulb located next to the fiber. Some light emitted from the bulb is trapped in the fiber and travels towards the meter. The light source chosen for this purpose is trivial, as long as the light emitted is constant. A light barrier is between the meter and light source.

A simple box with a hole for the fiber is sufficient for a light barrier. The light meter is located in the box. Some light will leak through the hole in the box, but the leakage can be accounted for by calibration of the test apparatus. This is a relative measurement, so leakage is simply a baseline. Locating the light meter far up or downstream from the box containing the light source will also reduce light

contamination of the light meter. A crack is indicated by a light pulse at the sensor.

### 3.2.1.2 Reflectivity

Mirror reflectivity is measured to maximize data collection of the active detector during the experiment. This QC checkpoint occurs after the fibers are mirrored, but before the fibers are inserted into the extrusion.

A technician connects the fiber to a light source and a light measuring device. A pulse of light is emitted from the source. The light travels down the fiber and bounces off the mirror and back to the light meter. The meter compares amount of light reflected off the mirror to the original light impulse. A mirror with 70% reflectivity is considered usable.

Fibers that fail the mirror reflectivity test do not necessarily need to be discarded. The fiber can be repolished and sputtered. Repolishing does not alter the fiber length substantially. The author does not know of any limit to the number of times a fiber can be mirrored.

### 3.2.2 Pressure Drop Test

The modules are pressure tested at two checkpoints during the assembly process. The first pressure test occurs directly before the modules are shipped from the factory to the mine. The second pressure test occurs after the modules are banded to the steel plane. The goal of the pressure test is to ensure the module is leak free before installing the module in the detector. This QC check is a simple test that monitors for gas leaks when the module has an internal pressure of 192 kPa (28 psig), which is four times the operating pressure of the experiment. Figure 3.8 is a flowchart of the test.

The methodology for the pressure test is straight forward. First, the modules are attached to an air pressure source using standard pressure fittings. An operator then increases the pressure inside the module to 4 times the performance pressure. This pressure limit provides a conservative factor of safety but is low enough so the module is not damaged. After the pressure reaches the test pressure, the technician isolates the module by closing a shut-off valve. The module is allowed to stabilize for 30 seconds, and then the pressure is monitored for several minutes by a pressure

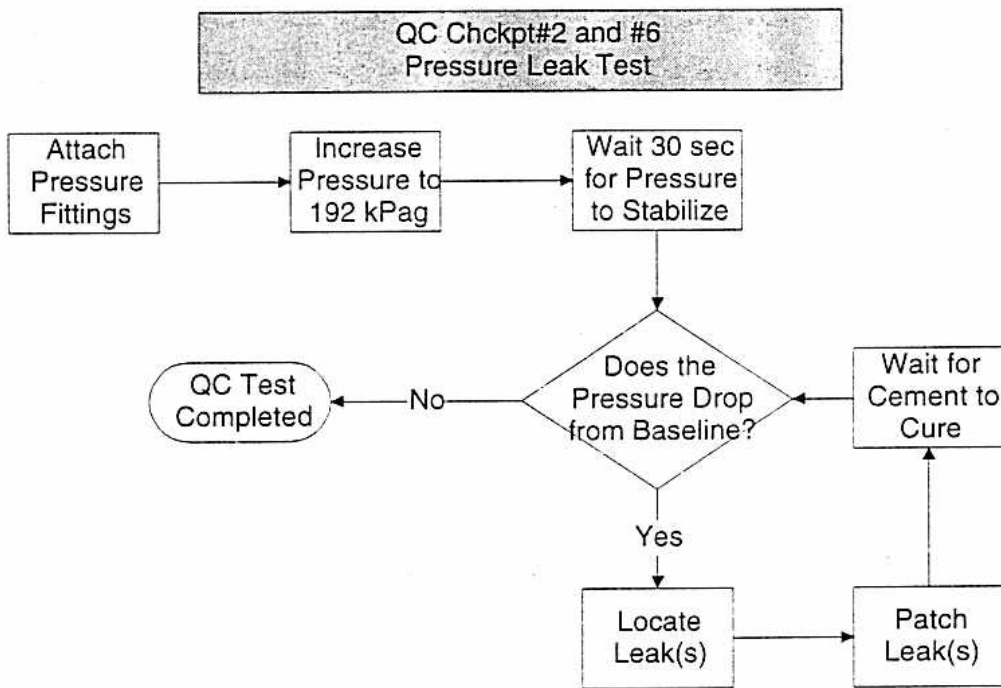


Figure 3.8: Flowchart Detailing the Second and Sixth Quality Control Checkpoints

transducer. A pressure drop greater than a tolerance value, yet to be determined, indicates a leak.

Modules that fail this test are salvageable. It is possible to patch any leaks using PVC cement. After curing, the module can undergo testing again. It is possible to locate leaks with soapy water.

### 3.2.3 Light Leaks

Light leaks can contaminate MINOS data. This QC checkpoint occurs directly before the module is placed on the steel plane and isolates any leaks. This test is necessary because any excess light that leaks into the module can mask the signal produced by an event. Figure 3.9 illustrates the light leak test procedure.

This test is straight forward and does not require any specialized equipment. First, the module is placed in a box. Next, the fibers are attached to a phototube, and a light wand is turned on inside the box. The operator sweeps the wand along the length of the box, and the fiber output is monitored by a phototube. A local maxima above a tolerance value on the phototube trace indicates the location of a thin spot or leak in the light barrier.

The operator can easily patch a module containing a leak. The operator simply wraps the cross section containing the leak with a strip of wide black tape. The exact location of the leak on the perimeter is not necessary because the tape should cover any leaks, and precisely locating a pinhole is too time consuming. After all the leaks are repaired, the module is retested.

### 3.2.4 Maintenance and Repair

The only structural items on the detector that can be repaired are the endcap and manifold seals. The bypass is inaccessible and, therefore, can not be repaired. If the bypass or any other inaccessible area leaks, the scintillator must be removed from the module. This module is then useless for the remainder of the experiment, since entire modules can not be replaced once installed.

Repairing small, seeping leaks is a quick and simple procedure. The surface is prepared with a solvent such as acetone or isopropanol. After removing the solvent, the

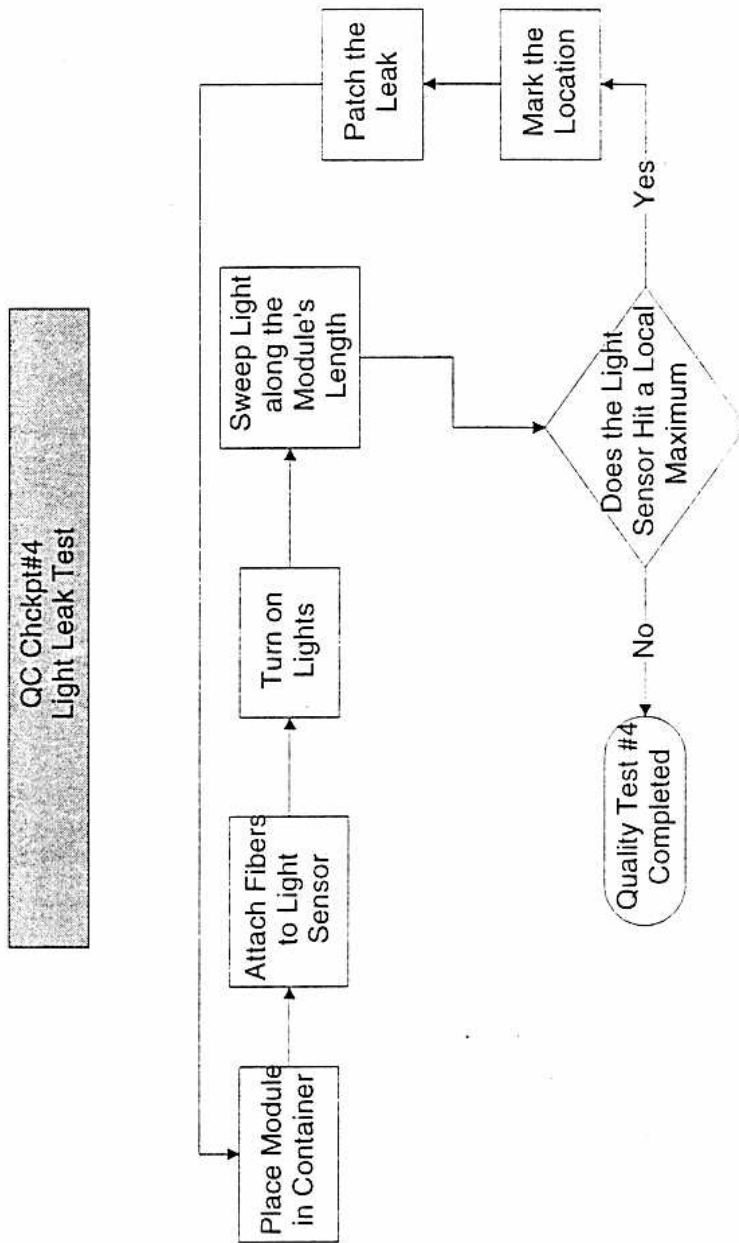


Figure 3.9: Flowchart Detailing the Fourth Quality Control Checkpoint

hole is covered with the same primer and cement described in section 3.1.2. The leak is sealed after the epoxy cures. This method does not require a "patch" or other sealing aid. This method only repairs leaks without back pressure. To repair leaks with back pressure, the scintillator must be removed from the module.

Two prototype modules with artificial leaks were repaired and leak tested using this method. The author made two slits, each approximately 0.32 cm (0.125 in) long, in a module with a razor blade and partially filled the modules with mineral oil. The oil slowly leaked from the extrusion and covered the outside of the module.

Each of the holes were sealed with a slightly different method. The oil was not cleaned off the opening of one hole, while isopropanol was used to clean the oil away from the other hole. Primer and cement were applied to the openings of both leaks. The modules were allowed to stand upright, so the scintillator inside the module would provide a head pressure that would continue to force scintillator out the razor blade hole.

The module was pressure tested after the cement cured. A 207 kPa (30 psig) internal pressure was placed in the module. The module was monitored for 10 minutes, and then the module was left without observation for 72 hours. The module maintained pressure during the initial 10 minute period. However, sometime during the subsequent 72-hour period the module lost all pressure. After fixing a leak on a fitting the module was pressurized to 50 psi and left in a water tank. After 1 hour the pressure had dropped to 40 psi, but the author could not determine the leak point. Air bubbles had formed around the endcap seal, but no bubbles were visible on the repaired areas. Thus, the test was not fully conclusive.

This method will not work when the module is under pressure. Scintillator under pressure exits in a stream and prevents the cement from closing the hole. To repair this case, the scintillator must be drained from the module before repairing the leak.

# Chapter 4

## Test Program

This chapter discusses the test program performed on the active detector design. The testing focused on four separate areas of the design. Section 4.1 presents the testing performed to measure the dimensional stability of the PVC extrusions. Section 4.2 describes the testing of the seal integrity. Section 4.3 discusses testing performed on the PVC cement used. Section 4.4 presents testing performed on the liquid scintillator.

### 4.1 Creep Testing

Resistance to creep is a major concern for the detector modules because MINOS is scheduled to run for more than 10 years. The module must not leak due to elongation of the PVC extrusion. Therefore, the modules were tested for dimensional stability while exposed to Bicron 517L and under a pressure load.

This section discusses the test program used to determine the stability of PVC when simultaneously exposed to liquid scintillator and stress. The first subsection presents deflection predictions and a preliminary creep analysis. The second subsection outlines the experimental creep test procedure. The third subsection presents the experimental test results and conclusions.

#### 4.1.1 Theoretical Behavior and Predictions

The behavior of the PVC extrusions under load was predicted by simple beam flexure models. The bow in the outer wall was modeled by simply-supported and double-fixed

end conditions. Figure 4.1 illustrates the geometry and end conditions used in the modeling process. The elongation of the wall, or web, was modeled as a bar in tension. Detailed deflection calculations are located in Appendix B. Cellular dimensions are also located in that appendix.

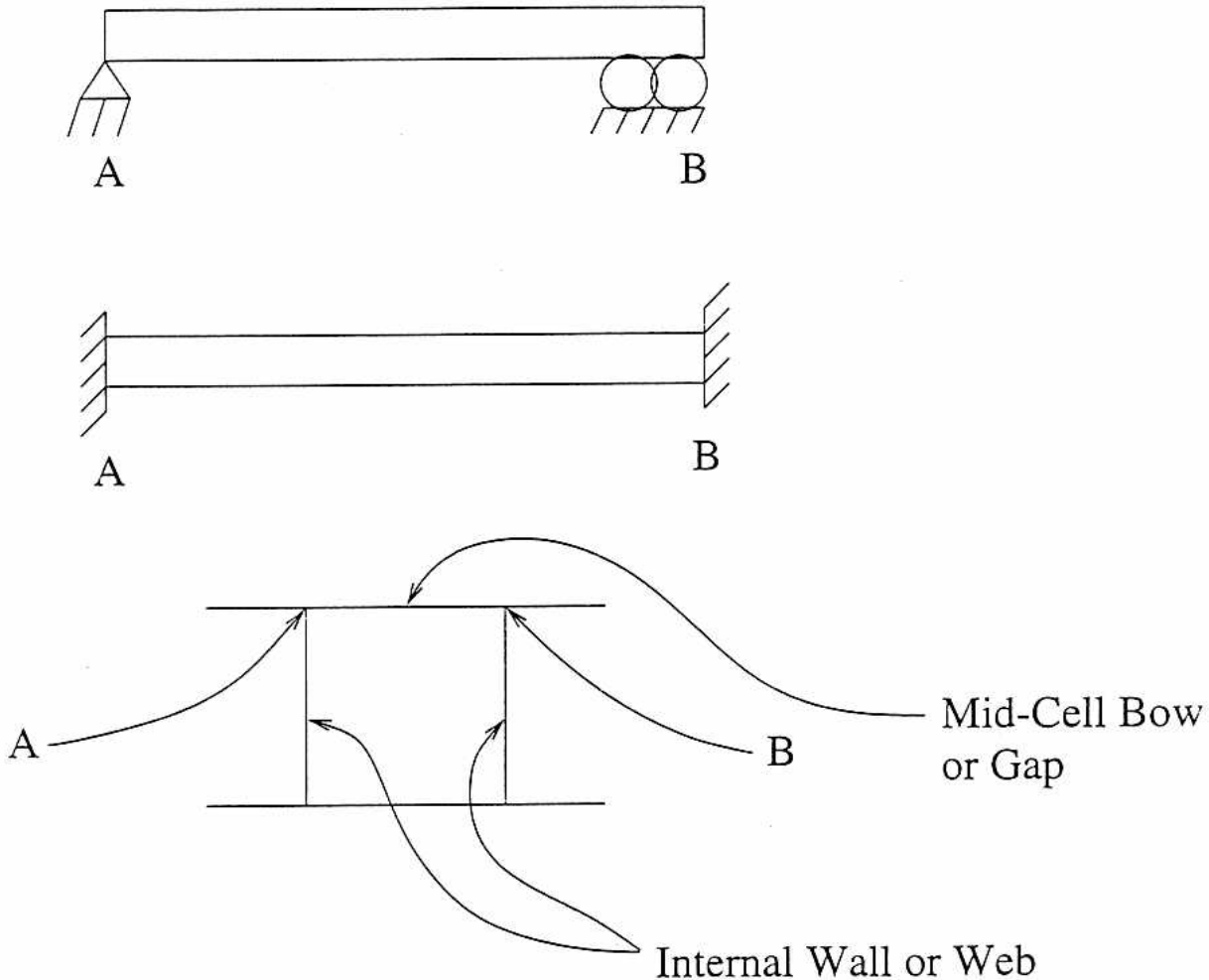


Figure 4.1: End Conditions Used in the Beam Flexure Models to Predict Creep

The model using simply-supported ends should over-predict the deflection at the mid-span of the gap. The deflection angle in this model starts at some maximum value at the wall and passes through an inflection point at the mid-point of the beam. In the actual extrusion, the deflection angle starts at zero, increases, and passes through inflection points at approximately one-quarter and three-quarters of the beam length.

The model does allow the end supports to move laterally towards each other as the beam flexes, which is consistent with the restraints of the actual model.

The simply-supported situation was also calculated by two different methods. The first method assumed a wide beam. The wide beam model is utilized when a beam is extremely deep in relation to length and thickness. In the wide beam model, the strain in the direction of depth is assumed to be negligible. The second method assumes a narrow beam. The narrow beam assumes plane stress.

The wide beam assumption reduces the deflection prediction by 9%. The total deflection predicted for the bow in the gap is  $3.3(10^{-4})$  m for 20°C and  $3.7(10^{-4})$ m for 45°C. This reduction of the predicted deflection occurs because for wide beams the material stiffness is reduced by:

$$\frac{1}{1 - \nu^2}$$

The prediction utilising the double fixed-end conditions are also reduced by 9%. For a more in depth discussion of wide beam modelling and analysis reference Roark and Young (1975).

Temperature affects the amount of deflection because the modulus of elasticity varies significantly with temperature. As the temperature is raised from 20°C to 45°C, the modulus of elasticity decreases from 2964 MPa to 2679 MPa. At 20°C, the total deflection at the mid-span of the gap is 0.38 mm. At 45°C the total deflection at the mid-span of the gap is 0.42 mm.

The deflection of the mid-span of the gap was also predicted with double-fixed end conditions, which should under-predict the actual deflection of the gap. The double-fixed end condition holds the lateral distance between the supports constant, which is not the case in the actual extrusion. This model does constrain the beam deflection angle to behave similarly to the actual extrusion's wall. At 20°C, the total deflection at the mid-span of the gap is 0.085 mm. At 45° C, the total deflection at the mid-span of the gap is 0.095 mm.

The inner wall of the extrusion was modeled as a bar in tension. At 20°C, the web should elongate 13  $\mu$ m. At 45°C, the wall should elongate 14  $\mu$ m.

The previous analyses are expected bounds for the experimentally measured deflection. The simply-supported end conditions should provide the upper bounds, while the double-fixed end conditions should provide the lower bound for the mid-cell bow. The prediction for the elongation of the inner wall should be on the same order of magnitude as the experimentally measured deflection.

Internal pressure alone should not cause the walls of the PVC extrusion to creep. The testing temperature is 45°C, while the glass transition temperature of PVC is above 81°C (Brandrup and Immergut, 1989). When a polymer is below the glass transition temperature, the polymer does not exhibit viscoelastic behavior (Ferry, 1980). Therefore, if any creep, or dimensional instability, is observed in the experimental data, the creep is evidence of chemical incompatibility between the scintillator and PVC.

#### 4.1.2 Test Procedure

The creep test monitored the deflection of several points on prototype extrusions over a 3000 hour period. The points monitored were on the outer surface of the PVC extrusion at the internal walls and the bow in the mid-cell gap. Fixing the prototype into a jig allowed the technician to measure the dimensional change with a dial caliper. Figure 4.2 shows the measurement locations on the module.

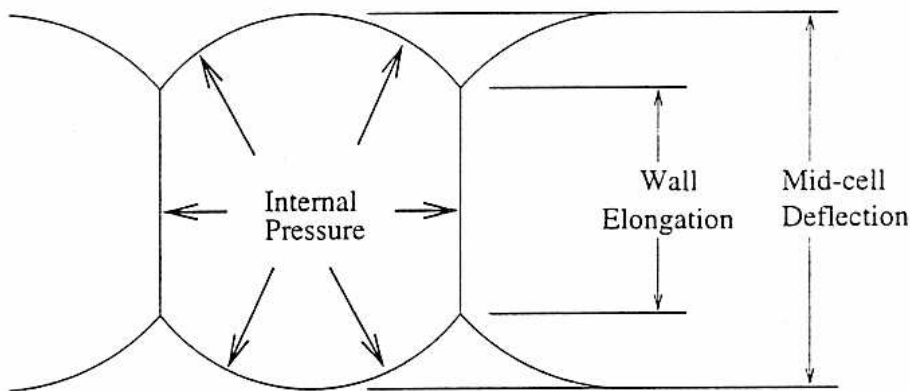


Figure 4.2: Measurement Locations for Creep Testing. The mid-cell deflection measurements shown in the figure are twice the results given in this thesis.

The extrusions were filled with scintillator and kept in an insulated container regu-

lated at 45°C between measurements. This temperature is roughly 25°C higher than the temperature in the mine, but below the temperature where the scintillator or PVC would degrade. The high temperature acts as an accelerant for any structural breakdown of the PVC due to interaction with the scintillator. The rate of acceleration is unknown, however. If creep is evident during the test, then the scintillator and PVC are most likely incompatible.

The extrusions were attached to a static pressure source of 145 kPa (21 psig). A pressure cylinder filled with nitrogen, which was regulated manually with a needle valve and pressure gauge, was the pressure source. The pressure is triple the operating pressure of 49.4 kPa (7 psig). The over-pressure, just as with temperature, acts as a creep accelerant. As previously stated, the PVC should not creep due to pressure or temperature.

#### 4.1.3 Experimental Results and Conclusions

Figure 4.3 is a graph that illustrates how the deflection of the web changed with time. The initial extrusion pressurization caused the wall to elongate approximately 0.15 mm. Over the course of the 3000 hour test, the elongation varied from 0.04 to 0.42 mm. The expected elongation is on the order of 15  $\mu\text{m}$ . The data is indicative of  $\pm 0.2$  mm repeatability in measurement.

Figure 4.4 is a graph that presents the change in deflection of the mid-cell gap over time. The gap deflected approximately 0.35 mm almost immediately after the pressure source was applied. After the initial expansion, the deflection ranged from 0.18 to 0.56 mm. The expected deflection is between 0.08 mm and 0.40 mm. The data is indicative of  $\pm 0.2$  mm repeatability in measurement.

Much of the fluctuation in deflection shown in both figures 4.3 and 4.4 might be due to errors introduced into the test. Even though the modules were kept at a constant temperature during the test, the modules were exposed to room temperature air for an unspecified time period before deflection measurements were made. After measuring, the extrusions were placed back into the heated container. Also, the measurement fixture did not require the extrusion to be measured at exactly the same points each time. Each of these effects will now be discussed in detail.

Some of the error was produced by temperature differences between extrusions. Before

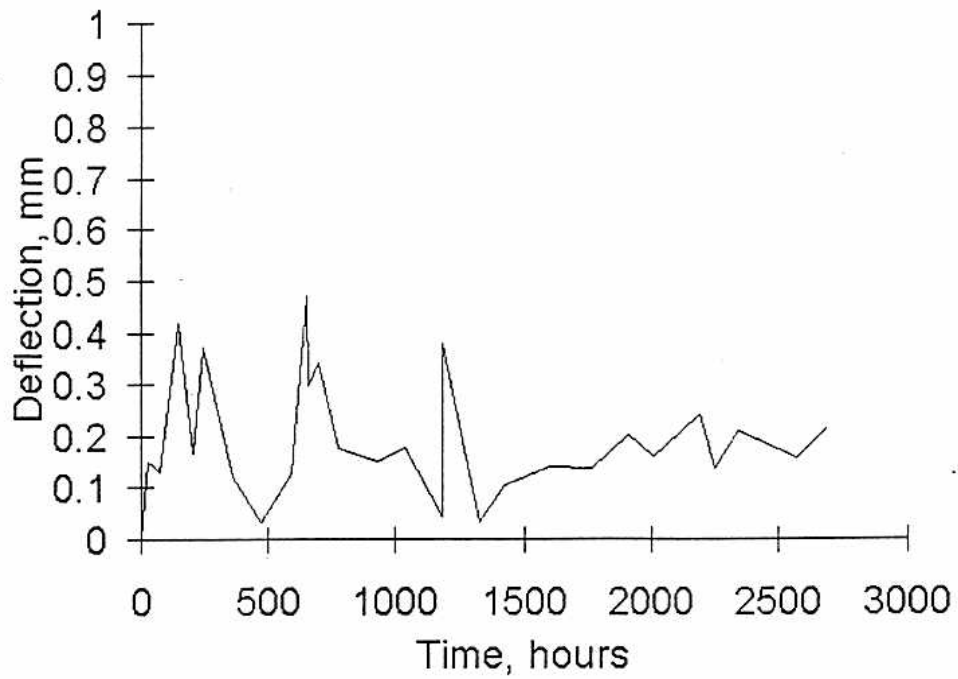


Figure 4.3: Change in Elongation of an Internal Wall of a PVC Extrusion over Time, Internal Pressure = 144.8 kPa, Wall Thickness = 1.0 mm, Scintillator = Bicron 517L

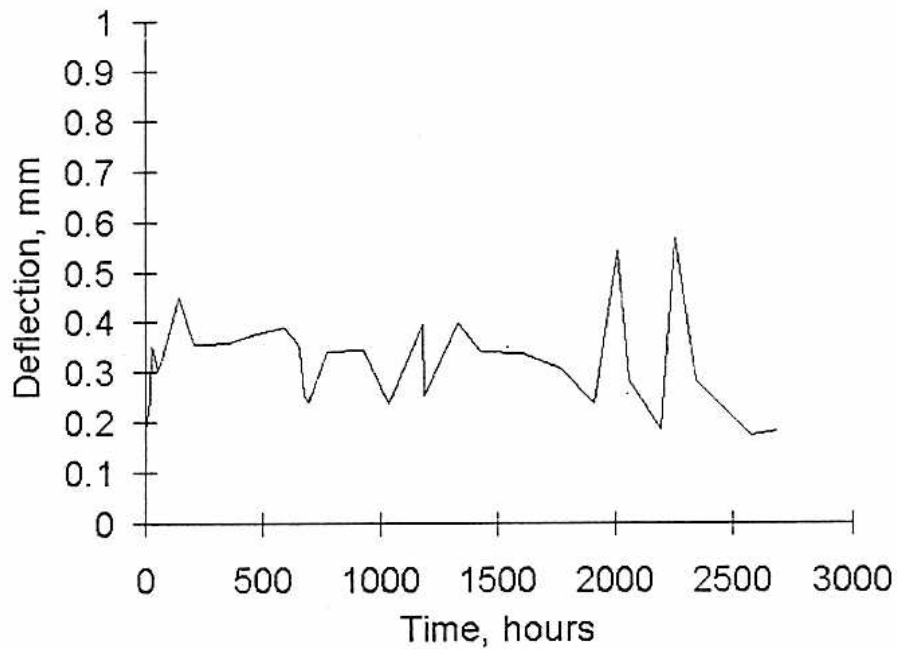


Figure 4.4: Change in the Mid-cell Bow in the Outer Wall of a PVC Extrusion over Time, Internal Pressure = 144.8 kPa, Wall Thickness = 1.5 mm, Scintillator = Bicron 517L

measurement, the extrusions were removed from the constant temperature environment in the insulated container. As the technician started taking measurements, the extrusions would cool causing the first extrusion to be warmer than the last. The test was also performed during the summer in a room without temperature control. If the extrusions were allowed to cool completely to the ambient temperature, the measurement temperature could vary by 20°C.

The deflection measurements were not always made in exactly the same location because of the measurement fixture. A mark on the surface of the extrusion was used to indicate the measurement location. Since the fixture did not have a "hard stop", the technician could only measure close to the mark, not on the exact spot. As shown in figure 4.2 many of the surfaces on the extrusion were rounded, exacerbating the repeatability problem. The small deflections measured also amplified the effects of errors.

The results of the creep test show that PVC is an acceptable base material for the active detector module. The scintillator, Bicron 517L, and PVC are chemically compatible. Figures 4.3 and 4.4 do not indicate creep. The curves have a mean slope that is approximately zero.

## 4.2 Seal Integrity Testing

Perhaps the most controversial area of the liquid scintillator detector is the seal designs. The seal must withstand the handling of the installation process and then remain leak-free for the entire experiment, while requiring little or no maintenance. To determine the integrity of the seal, a battery of tests were performed on both the bypass and end cap seal designs.

The following few sections discuss the four tests performed on the seal. The first section describes burst testing. The second section discusses impact testing. The third section describes pressure cycle testing. The fourth section describes thermal cycle testing.

### 4.2.1 Burst Testing

Before performance testing the prototype seals, the author thought it necessary to find the maximum pressure the seals and PVC extrusion could withstand. The maximum

pressure is used to set safety limits for the remainder of the testing.

The following three sections present the test method and experimental data. The first section describes the test procedure. The second section presents the results of the test. The third section discusses some conclusions about this test.

#### 4.2.1.1 Burst Test Procedure

Small prototype modules were tested to failure. After the sealant cement achieved full cure, greater than 48 hours for this material, the modules were attached to a static pressure source. The extrusions and seals had not been tampered with in any way, so the modules were assumed to be in pristine condition.

The pressure in the module was ramped up slowly, so any failures could be immediately observed. The pressure was increased in 69 kPa (10 psig) steps and then held for 30 seconds, which allowed the modules to stabilize. If no failure was observed, the pressure was increased again.

#### 4.2.1.2 Burst Test Experimental Results

Figure 4.5 is a bar chart of the various burst and failure pressures for the end cap and bypass seals. For the end cap tests the extrusion failed at 690 (100 psig), 760 (110 psig), and 830 kPa (120 psig) for -20°C, 20°C, and 50°C, respectively. The bypass seal was only tested at 20°C and failed at 620 kPa (90 psig).

The bypass and end cap seals failed by different modes. In every end cap trial, the extrusion burst before the end cap seal failed. The failure mode for the bypass trials was a leak through the seal.

When the PVC extrusion failed, it failed explosively. The failure started at the point where a web joined the outer wall, usually towards the end of the extrusion having the end cap seal. At the time of failure, a crack propagated along the web until much of the outer wall had separated. The outer wall then shattered laterally along the center of the extrusion. While the extrusion was destroyed, the end cap seal remained intact in all but one case.

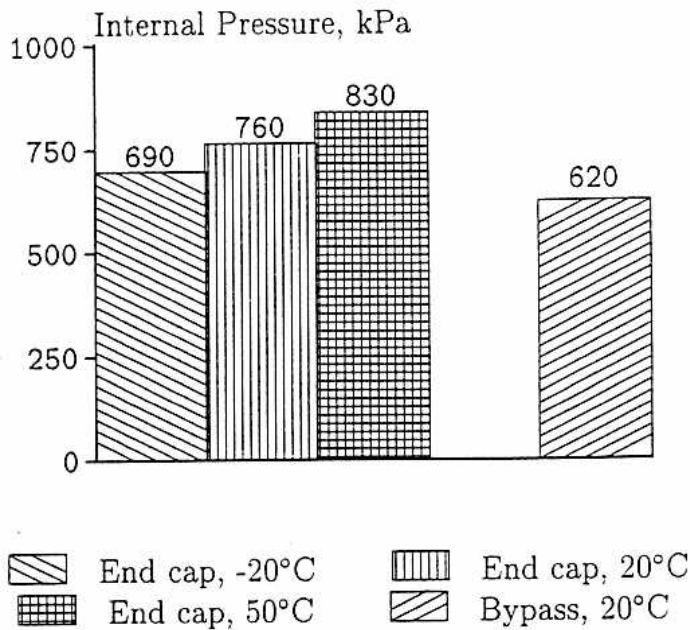


Figure 4.5: Burst Pressure of Active Detector Prototypes

#### 4.2.1.3 Burst Test Conclusions

The seal designs for both the end cap and bypass will not fail when the active detector modules are initially filled with scintillator. The failure pressure for the bypass, which is the weakest seal design in the active detector, is 12.5 times higher than the static pressure in an actual module.

The extrusion strength increases with temperature. The end cap seal design was tested at three different temperatures. The burst pressure increased with each increase in temperature. This result is intuitively correct because PVC becomes more elastic as temperature is increased. Therefore, at lower temperatures the PVC extrusion will not withstand as high a strain rate as at higher temperatures. This trend should continue until the temperature is at least equal to the crystallization temperature.

#### 4.2.2 Impact Testing

During the assembly and handling of the modules, potential for impact or shock loading of the modules exists. A material handler may drop the module, or perhaps an assembler may drop a tool onto a module. In either of these two cases, the module must remain liquid-tight.

The following sections discuss impact testing performed on small prototype modules. The first subsection describes the test procedure. The second subsection presents the experimental test results. The final subsection discusses the conclusions drawn from the testing.

#### 4.2.2.1 Impact Test Procedure

The impact strength of the prototypes were tested in three locations. The three locations are the outer wall of the PVC extrusion, the middle of the end cap, and the end of the bypass. Figures 4.6, 4.7, and 4.8 are drawings showing the location of the impact. The test process for each target was identical.

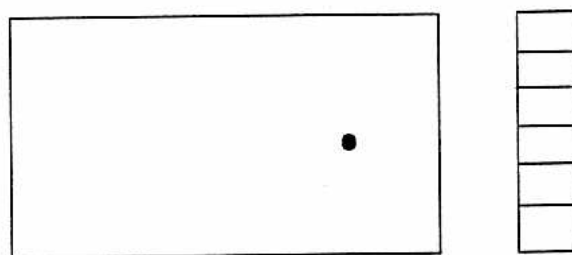


Figure 4.6: Impact Location on the Extrusion

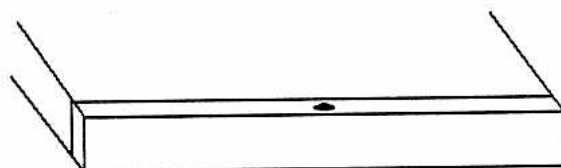


Figure 4.7: Impact Location on the End cap

A 12.7 mm (0.5 inch) rod delivered the impact to the prototype module. The rod, which had weights attached to the top and ran through a guide tube, was dropped a specified distance onto the appropriate target on the module. The module was fixed to a table by C-clamps.

After impact, the module was attached to a pressure source. The pressure was increased in 69 kPa (10 psig) steps. At each step, the pressure was held for 30 seconds.

Target	Temperature	Impact Energy	Impact Pressure	Result
	°C (°F)	N-m (ft-lbf)	N-m/cm <sup>2</sup> (lbf-ft/in <sup>2</sup> )	
End cap	18 (65)	54 (40)	43 (203)	No Failure
End cap	-20 (-4)	54 (40)	43 (203)	No Failure
End cap	-20 (-4)	99 (73)	78 (370)	No Failure
Bypass	18 (65)	54 (40)	43 (203)	No Failure
Bypass	18 (65)	99 (73)	78 (370)	Leak at 370 kPa (60 psig)
External Wall	18 (65)	20 (15)	16 (76)	No Failure
External Wall	18 (65)	27 (20)	21 (100)	Wall Punctured

Table 4.1: Impact Strength of End cap and Bypass Seal Designs, Maximum Internal Pressure = 480 kPa (70 psig)

Source	Impact Energy	Impact Pressure
	N-m (ft-lbf)	N-m/cm <sup>2</sup> (lbf-ft/in <sup>2</sup> )
20 Oz. hammer dropped 3 feet	5.1 (3.8)	1 (4.8)
One end of module dropped 4 feet	136 (100)	7.6 (35.8)
Entire module dropped 4 feet onto one end	270 (200)	15.1 (71.8)

Table 4.2: Typical Impact Load That May Occur During Installation

an order of magnitude larger than that of the rod used during testing. Based on impact pressure, the test impacts were more severe.

A principle of impact pressure is explained with a simple analogy. Two objects are dropped the same distance, waist height, onto the reader's bare foot. Both objects weigh 44.5 N (10 lbf) and are rigid, but have different impact areas. The first object has a footprint about the size of a pad of paper; the other has the diameter of a pencil and is long and slender. Which object punctures the reader's foot?

### 4.2.3 Pressure Cycle Testing

During assembly and installation, the active detector modules will undergo several pressure cycles. Two pressure cycles are from quality control tests. The final pressurization happens when the modules are finally installed in the mine and filled with scintillator.

A prototype module was cycled through several high and low pressure periods in a modified fatigue test. The object of the test was not to determine the ultimate number of cycles to failure, but simply to produce a level of confidence in the design. The pressure was cycled from atmospheric to 410 kPa (60 psig).

The module underwent a total of 30 pressure cycles. After 20 cycles, the module sat overnight with an internal pressure of 410 kPa (60 psig). The remaining 10 cycles were applied the following day. The module was monitored for leaks throughout the test; none developed. The pressure was ramped up and down in the same manner as in the impact and burst tests.

The small number of pressure cycles applied to the active detectors during the actual experiment are not expected to cause any problems. This test not only cycled the modules ten times more than expected, but the test also utilized a peak pressure exceeding the expected operating pressure by a factor of eight.

### 4.2.4 Thermal Cycling Testing

During the winter, the modules will undergo several thermal cycles, since the modules are assembled away from the mine. The modules are expected to be exposed to at least two cycles, in loading and unloading from the plant to a cold truck and then from the truck to the warm mine. The adhesive used in the seal could develop cracks induced from thermal stresses.

Three prototype modules were cycled through alternating environments of  $-20^{\circ}\text{C}$  ( $-4^{\circ}\text{F}$ ) and  $50^{\circ}\text{C}$  ( $122^{\circ}\text{F}$ ). The maximum temperature is probably realistic for a truck sitting in the summer sun on a hot summer day, but the lowest temperature a module might encounter is probably  $-40^{\circ}\text{C}$  ( $-40^{\circ}\text{F}$ ) during winter. The lower test temperature was limited by the freezer used. Each module was cycled through each temperature 15 times. The modules were kept in each environment for approximately an hour, to allow the module's temperature to stabilize.

After the thermal cycling, each module was leak tested. The pressure was ramped up to 480 kPa (70 psig) in a similar manner as for the burst test and held for a period of time. None of the modules leaked during the pressure test.

### 4.3 Adhesive Testing

A series of tests was performed to measure the strength of the adhesive used in both the end cap and bypass seals. The first test attempted to determine how the strength and stiffness of the adhesive change when exposed to the liquid scintillator, Bicron 517L. Another test measured how adhesive strength changed with cure time.

This section describes adhesive material property tests performed on the PVC cement used to seal the joints of the module. The first subsection describes a series of tests that measured the chemical compatibility of the adhesive and the liquid scintillator. The second subsection presents a series of tests that measured the bond strength of the adhesive joint over the curing time.

#### 4.3.1 Chemical Compatibility Testing

The structural integrity of the seals must not decline over the course of the MINOS experiment. Since the adhesive provides most of the strength to the seal joint, the liquid scintillator and the adhesive must be compatible.

The following two sections describe a test that checked the chemical compatibility of the adhesive and scintillator. This section first describes the test procedure. Next, the experimental results are presented along with conclusions about the data.

##### 4.3.1.1 Test Procedure

This test measured the change of the tensile and shear strengths of the adhesive. Figure 4.9 is a picture of the test specimens used in the tensile and shear tests. The tensile specimens bond two strips of PVC end-to-end in a butt joint, while the shear specimens utilize a lap joint.

Strength is dependent on the combination of the gap between strips and the amount of adhesive used. A jig held the strips during the curing process. The jig assured the gaps between the strips were as uniform as possible. All samples cured for the full

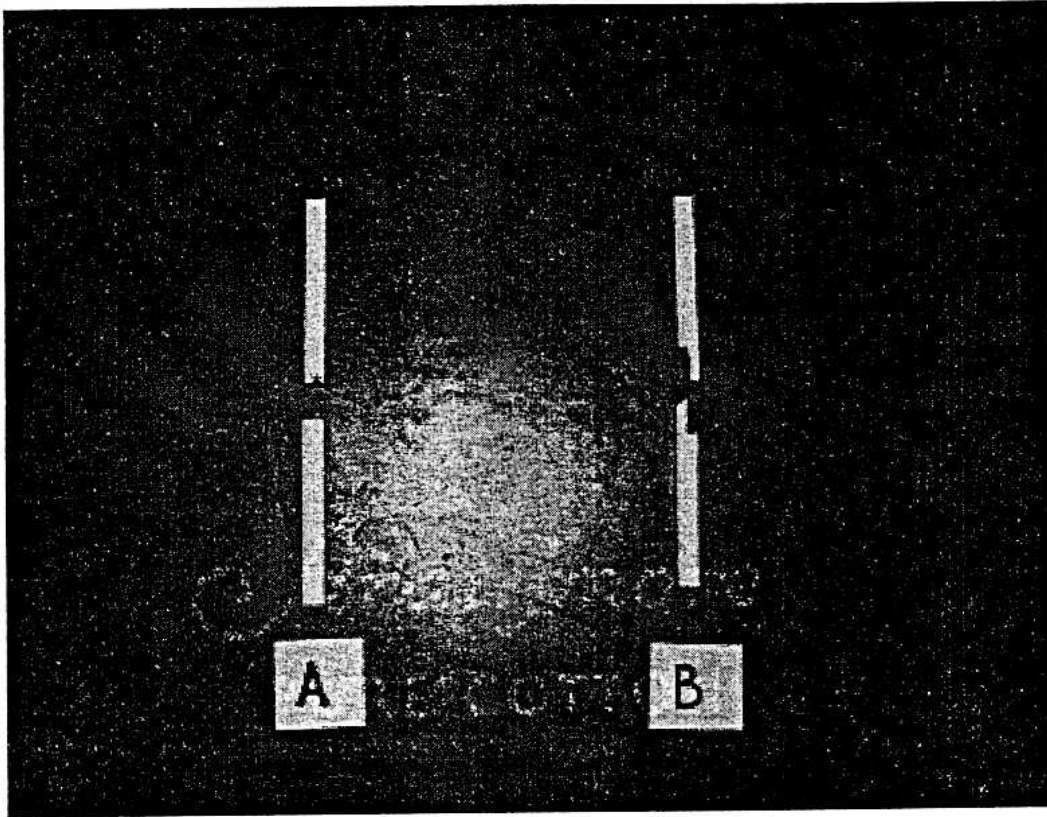


Figure 4.9: Tensile and Shear Adhesive Test Specimens, A) Tensile, B) Shear; Both sets have been tested to failure.

48 hours recommended by the manufacturer. At least nine specimens were tested for each exposure and joint type. However, only data for four of the tensile specimens for the two week exposure are reported in this document.<sup>1</sup>

After curing, three batches of strips were exposed to Bicron 517L for varying lengths of time. Each batch contained a set of tensile and shear test specimens. The first batch was a control and was not exposed to scintillator. The other batches were submerged in scintillator held at 45°C (113°F). One batch was exposed for 2 weeks or 336 hours. The second batch was exposed for 4 weeks or 672 hours. Just as with some of the previously described tests, the elevated temperature is assumed to be an aging accelerant.

The specimens were tensile tested after being removed from the scintillator and being allowed to dry. Figure 4.10 is a picture of the test machine and fixturing apparatus. The reader should note that the specimens are not gripped by the gripping jaws; rather a pin arrangement holds the strips.

The pin fixture eliminates most of the moment in the adhesive joint that can be created by a jaws-type fixture. The jaws hold the samples in a fixed position, so if the test sample is not coaxial with the tensile machine, a moment is created in the joint. Figure 4.11 is an illustration of this phenomena. Allowing the moment will introduce shear stress into the tensile stress test or vice-a-versa. The pin arrangement helps ensure application of a pure tensile force. Figure 4.12 is a sketch of the pin fixture.

#### 4.3.1.2 Experimental Results

Figures 4.13, 4.14, 4.15, and 4.16 contain the results of the chemical compatibility tests. Each table contains the mean and standard deviation for the ultimate stress and modulus. The upper and lower limits presented below represent the  $\pm 3$  standard deviation tolerance interval. Each of the graphs contains four items of information: the actual test data points for each test parameter, the averaged stress or modulus, the  $(+)3\sigma$  upper limit, and the  $(-)3\sigma$  lower limit.

The tensile properties do not change with exposure time. The ultimate stress for all tensile specimens is approximately 15 MPa (2.2 ksi). The upper and lower  $3\sigma$  limits for the control group are 20 MPa (2.9 ksi) to 8.4 MPa (1.2 ksi). The mean modulus

---

<sup>1</sup>Some data was lost due to a computer problem.

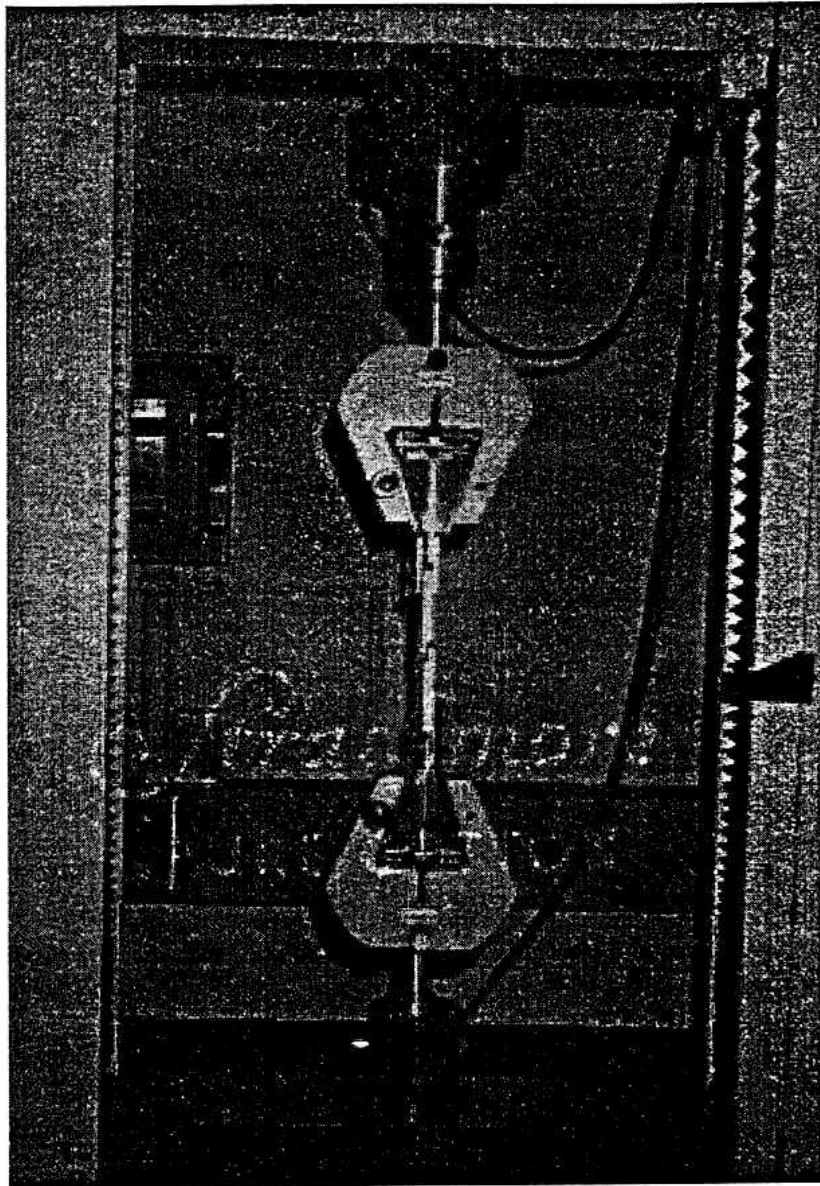


Figure 4.10: Photograph of the Testing Apparatus Used for the Tensile and Shear Tests

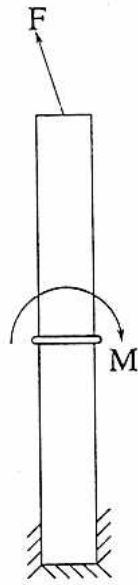


Figure 4.11: Illustration of the Moment Created in a Test Sample not Aligned with the Direction of Force

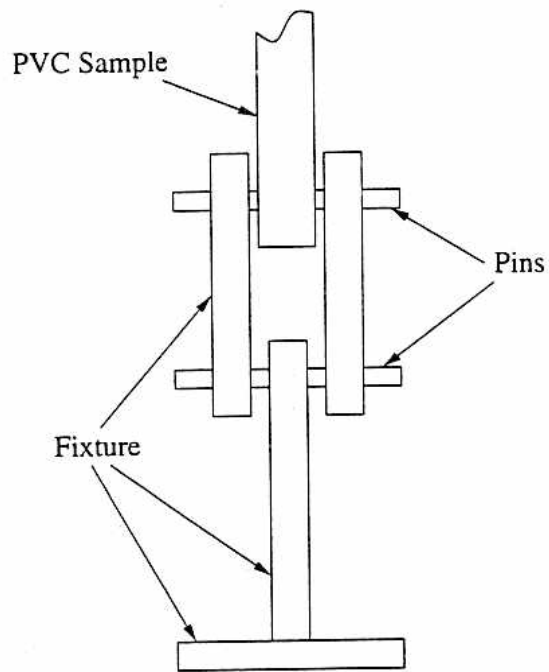


Figure 4.12: Sketch of the Pin Fixture

of elasticity for each group is approximately 750 MPa (108.8 ksi). The  $3\sigma$  tolerance interval for the control ranges from 569 MPa (82.6 ksi) to 883 MPa (128.2 ksi). The data for all three exposure times overlap, so no evidence for interaction between the scintillator and PVC exist.

The shear strength also does not change with exposure time. The tolerance intervals for the ultimate shear strength overlap between all three cases. The tightest interval is for the 672 hours exposure with bounds of 7 MPa (1.0 ksi) and 9.9 MPa (1.4 ksi), while the 336 <sup>hour</sup> ~~week~~ exposure had the widest interval with bounds of 4.9 MPa (0.71 ksi) and 11.1 MPa (1.6 ksi). The control batch had the widest interval for the modulus of rigidity with bounds of 185.4 MPa (26.9 ksi) and 535.5 MPa (77.7 ksi). All three intervals for the modulus overlapped with each other.

Figure 4.17 and figure 4.18 are graphs of the response for the tensile and shear tests. The plots are representative for all exposure times. The tensile specimens are characterized by a linear rise until the ultimate stress, after which the specimen quickly fails. The adhesive does not yield in the tensile stress state. The shear specimens had a nonlinear elastic portion prior to the ultimate strength.

The stress-strain curve is characterized by distinct sections: backlash, elastic deformation, and plastic deformation. The failure point is included in the plastic deformation portion of the curve. This general form for the stress-strain curve is representative for all stress-strain curves given in this thesis.

The first section of the stress strain curve is caused by backlash. The backlash is mainly due to the pin fixture used to hold the samples. In order to install a sample into the fixture, the dowel pin holes in the fixture must be slightly closer together than the corresponding holes in the sample. Therefore, after the sample is in place the sample is loose or even under a slight compression load. The initial low slope section of the stress-strain curve is indicative of the slow elimination of this slack.

The second section for the tensile-specimen, stress-strain curve is linear elastic deformation. This portion of the curve occurs after the backlash is removed from the fixture. This section is typical for many materials and will not be discussed in detail.

The final section of the stress-strain curve is plastic deformation. In the beginning of this section, the stress level in the material continues to rise. After the ultimate engineering stress is reached, the material loses strength until the fracture occurs.

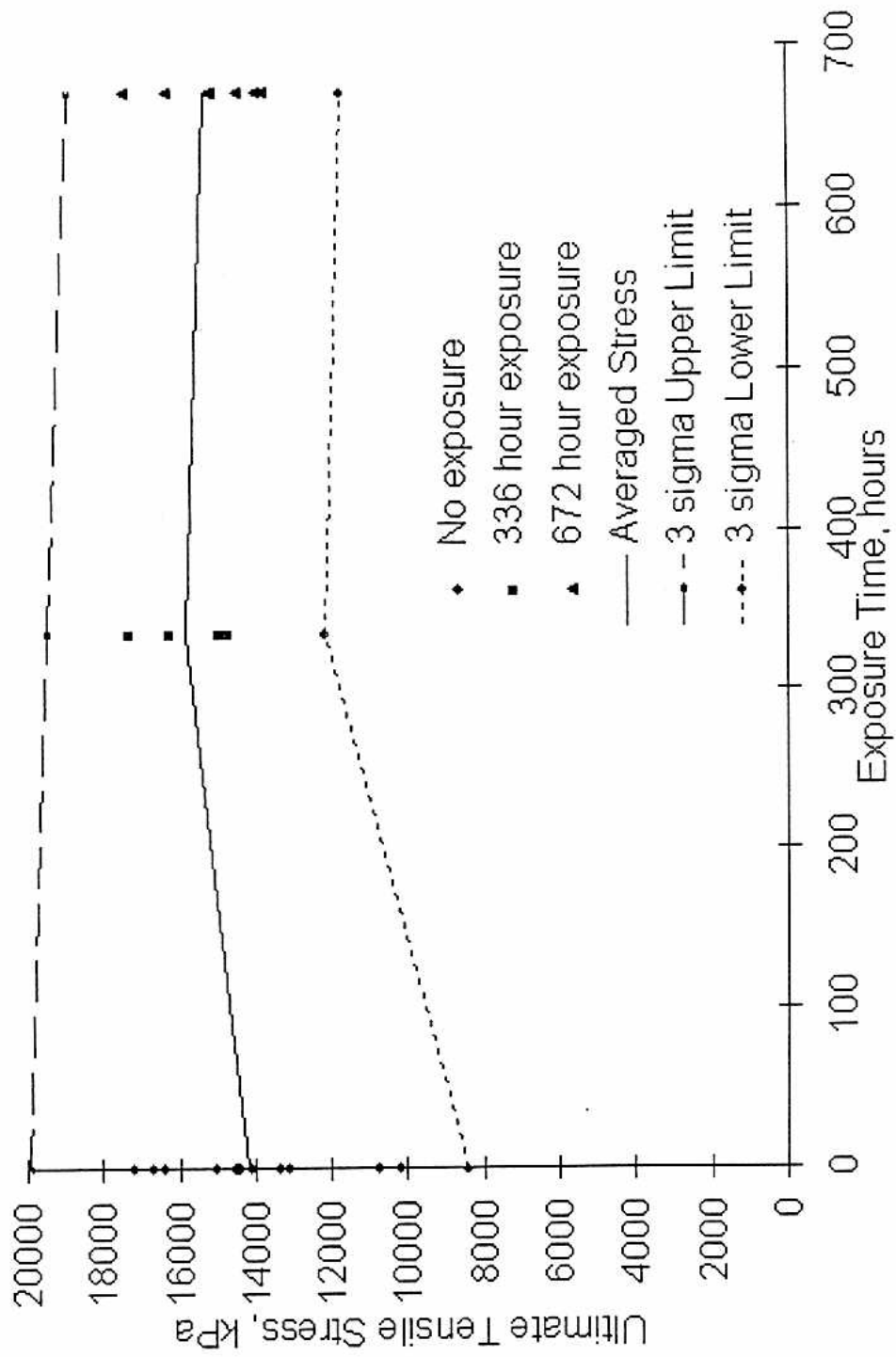


Figure 4.13: Affect of Bicorn 517L on the Ultimate Stress of the PVC Cement, Exposure at 45°C

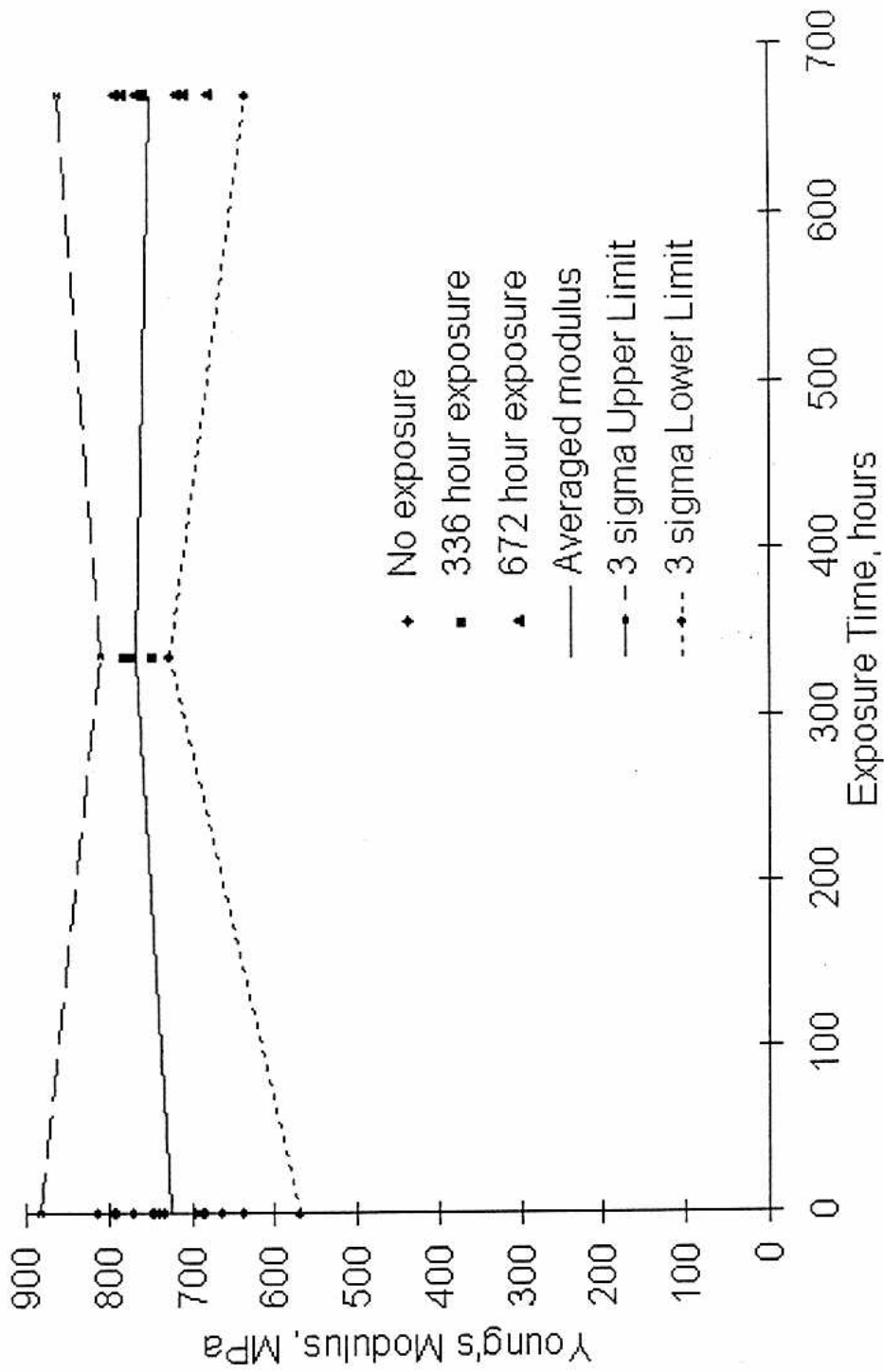


Figure 4.14: Affect of Bicron 517L on the Modulus of Elasticity of the PVC Cement, Exposure at 45°C

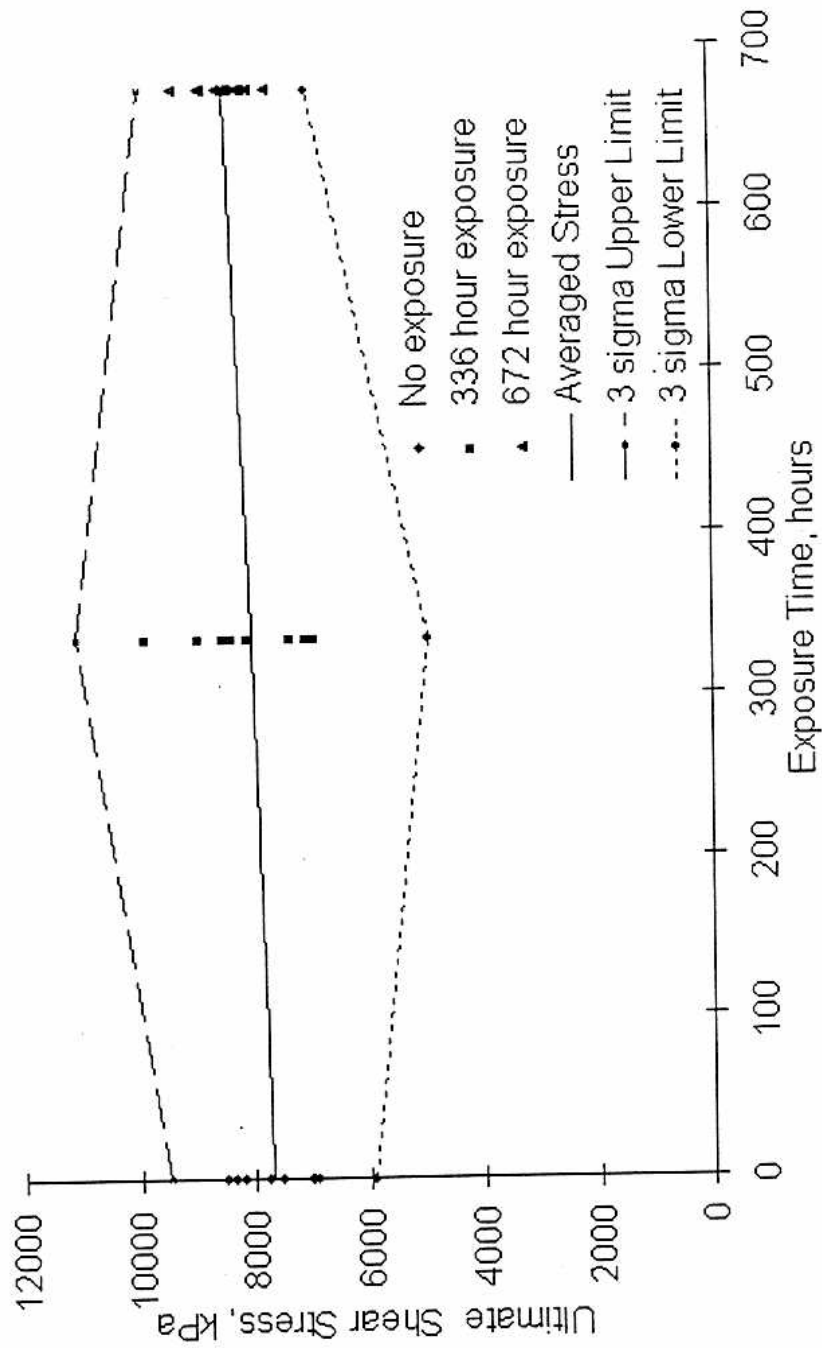


Figure 4.15: Affect of Bicorn 517L on the Ultimate Shear Stress of the PVC Cement, Exposure at 45°C

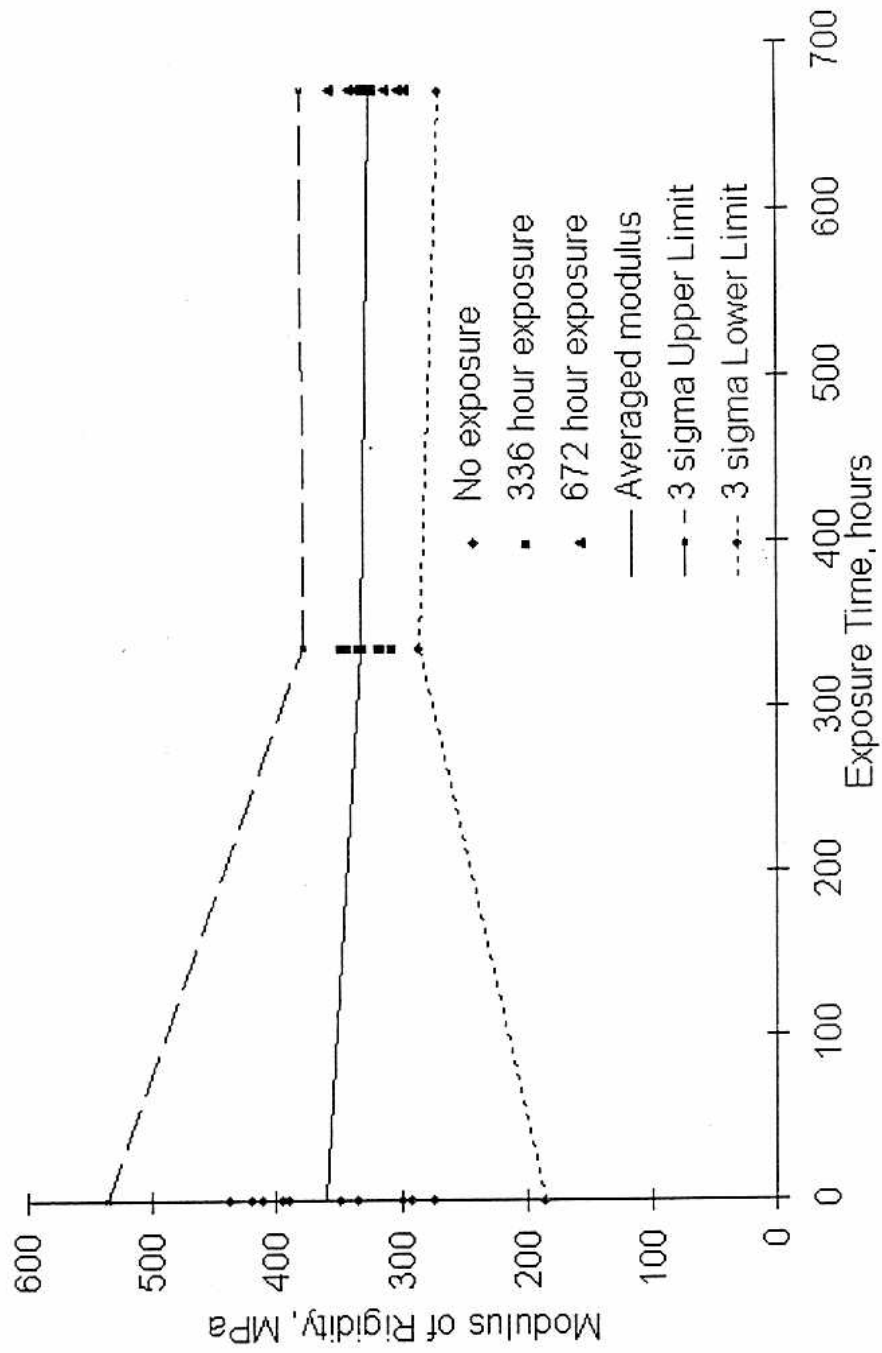


Figure 4.16: Affect of Bicron 517L on the Modulus of Rigidity of the PVC Cement, Exposure at 45°C

During plastic deformation, the material begins to neck. The necking reduces the load carrying area of the sample, and consequently the load strength of the material decreases.

Yielding in shear occurs at the bond interface between the adhesive and PVC strip and also in the adhesive itself. As the test sample is stressed, the sample elongates. At the low forces involved with these tests, the majority of the elongation is from the joint. When the sample nears the ultimate stress of the joint, the adhesive starts to peel off the PVC strips. When a significant portion of the bond is broken, the joint quickly loses rigidity, and the piece fails.

The yielding of the shear pieces is also evident upon forensic examination of the tensile and shear specimens. The tensile pieces always failed cleanly and would snap when failure occurred. The tensile failures occurred at either the bond interface or in the adhesive itself with no significant favoritism for either method. The shear pieces rarely made a sound at failure. Several pieces even remained attached by thin strands of adhesive.

The adhesive and liquid scintillator are chemically compatible. The data does not provide evidence for a change in tensile strength or shear strength or rigidity over the course of the test.

#### **4.3.2 Cure Period Testing**

The adhesive requires a full 48 hours before curing fully. This requirement would force the assemblers to have a large stockpile of in-process modules sitting idle while curing. However, idle modules consume costly floor space. In order to minimize expensive warehousing of modules, it is desirable to handle and test the modules before the adhesive cures completely. However, differences between the 48 hour cure specimens and the control groups discussed in section 4.3.1.2 were observed; these differences are discussed in section 4.3.2.2.

The cure period testing procedure is similar to the chemical compatibility testing described previously, except for the length of cure and the exposure to scintillator. The test samples are divided into three batches, a control with a full cure, a batch with 16 hours of cure, and a batch with 32 hours of cure. None of the specimens were exposed to scintillator.

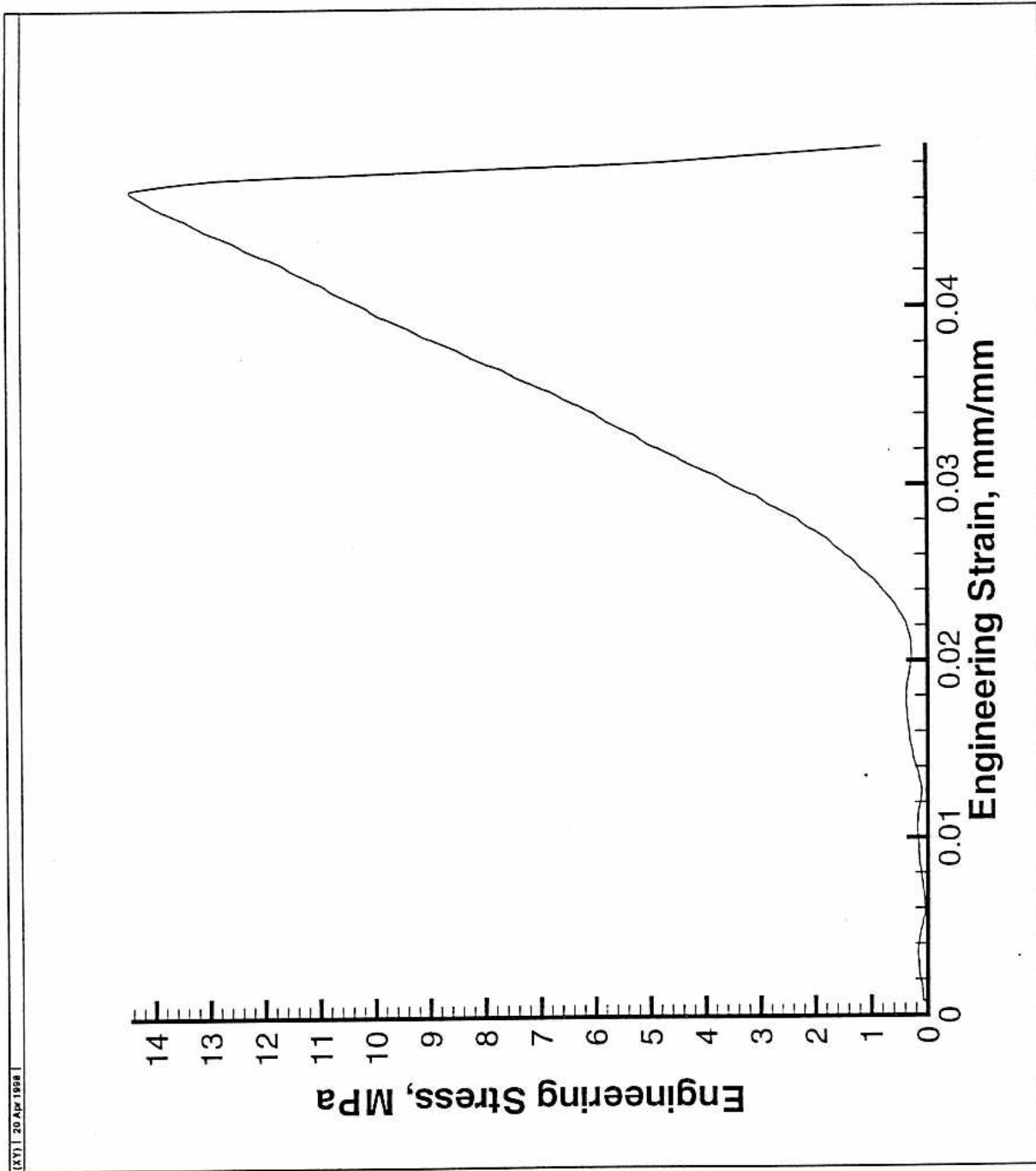


Figure 4.17: Typical Adhesive Stress-Strain Curve for a Tensile Specimen

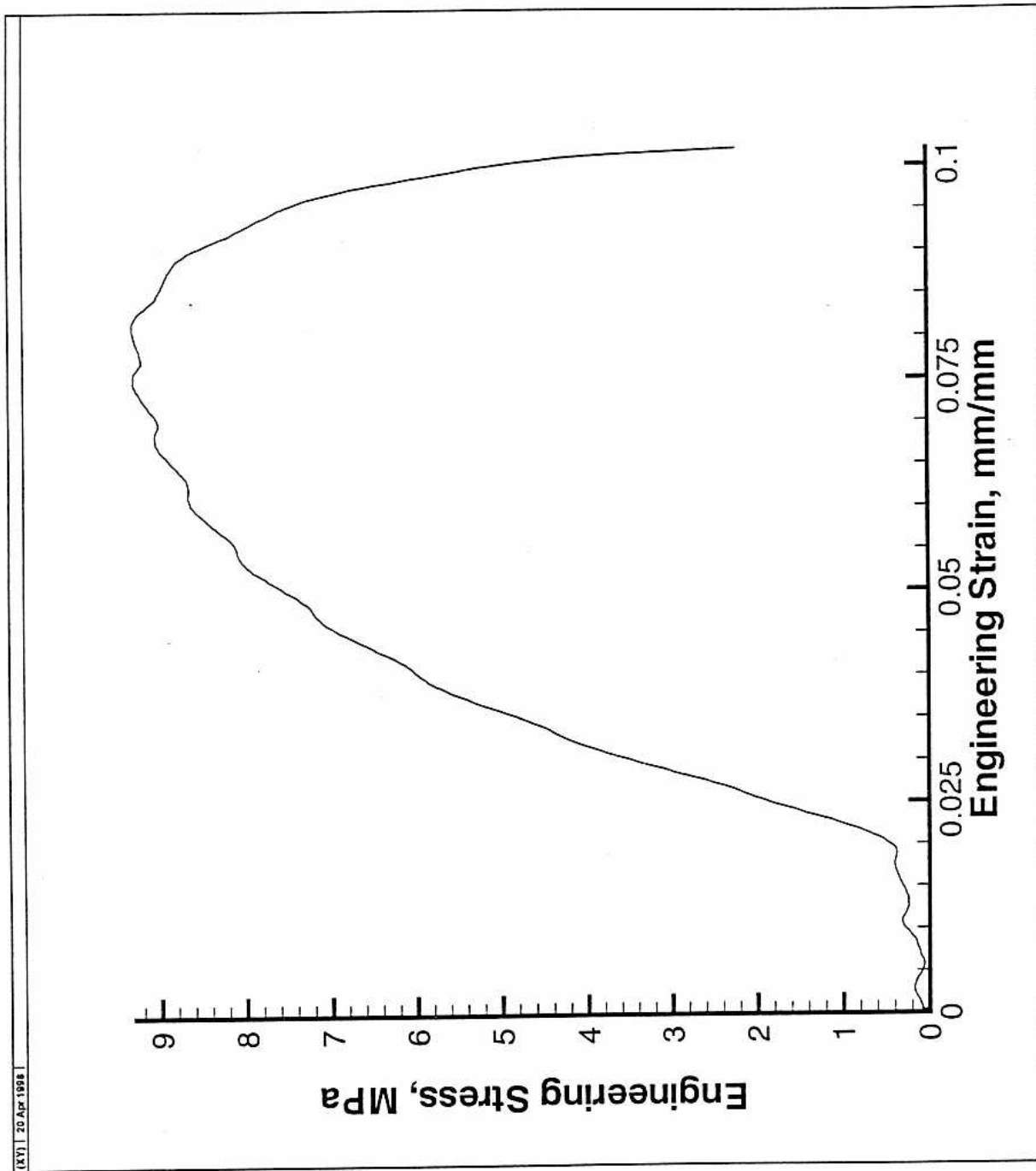


Figure 4.18: Typical Adhesive Stress-Strain Curve for a Shear Specimen

#### 4.3.2.1 Experimental Results

This section discusses the experimental results of the cure period property testing. Samples were tested for tensile and shear strength at three evenly spaced intervals during the curing process. Trends for the increase in rigidity and strength were constructed from the test data. The results of the tensile tests are discussed first. After the tensile results, the shear test results are presented.

**4.3.2.1.1 Tensile Properties During the Cure Period** Figure 4.19 contains a curve indicating the ultimate tensile strength, and figure 4.20 contains a curve for Young's modulus. The ultimate stress rises from 3500 to 6900 kPa (500 to 870 psi) during the 32 hour period starting at 16 hours and ending at full cure. The Modulus of Elasticity rises from 300 to 440 MPa (43.5 to 63.9 ksi). The data is scattered for each time sample.

Ultimate strength and Young's modulus have similar time-dependent characteristics during the curing cycle. Over the 48 hour cure period, both properties increase in an "S"-like curve. At the time of application (zero hours of cure), the PVC cement has a non-zero, yet negligible strength. As the cure period progresses, the cement quickly hardens.

Figures 4.19, 4.20, and 4.21 provide evidence that the time dependent properties plateau in the middle of the cure period then increase towards the end of the cure process. Each of these graphs show a greater increase in strength or stiffness, depending on the figure, for the 32 to 48 hour period than the 16 to 32 hour period. Testing at shorter time intervals than 16 hours will provide more insight into the time-dependent nature of the adhesive. Figure 4.24 in section 4.3.2.1.2 also provides evidence for a plateau in the time-dependent properties.

Figure 4.21 contains the stress-strain curve for the adhesive strength at 16, 32, and 48 hours of cure. Each curve contains three similar sections. The three sections are backlash, linear elastic deformation, and plastic deformation. Backlash is discussed in section 4.3.1.2.

Figure 4.21 provides evidence that the adhesive increases in stiffness more in the last 16 hour portion of cure cycle than the middle 16 hour portion. From 16 to 32 hours of cure, the  $\sigma_{ult}$  increases 22 percent, while  $\sigma_{ult}$  increases 55 percent from 32 to 48

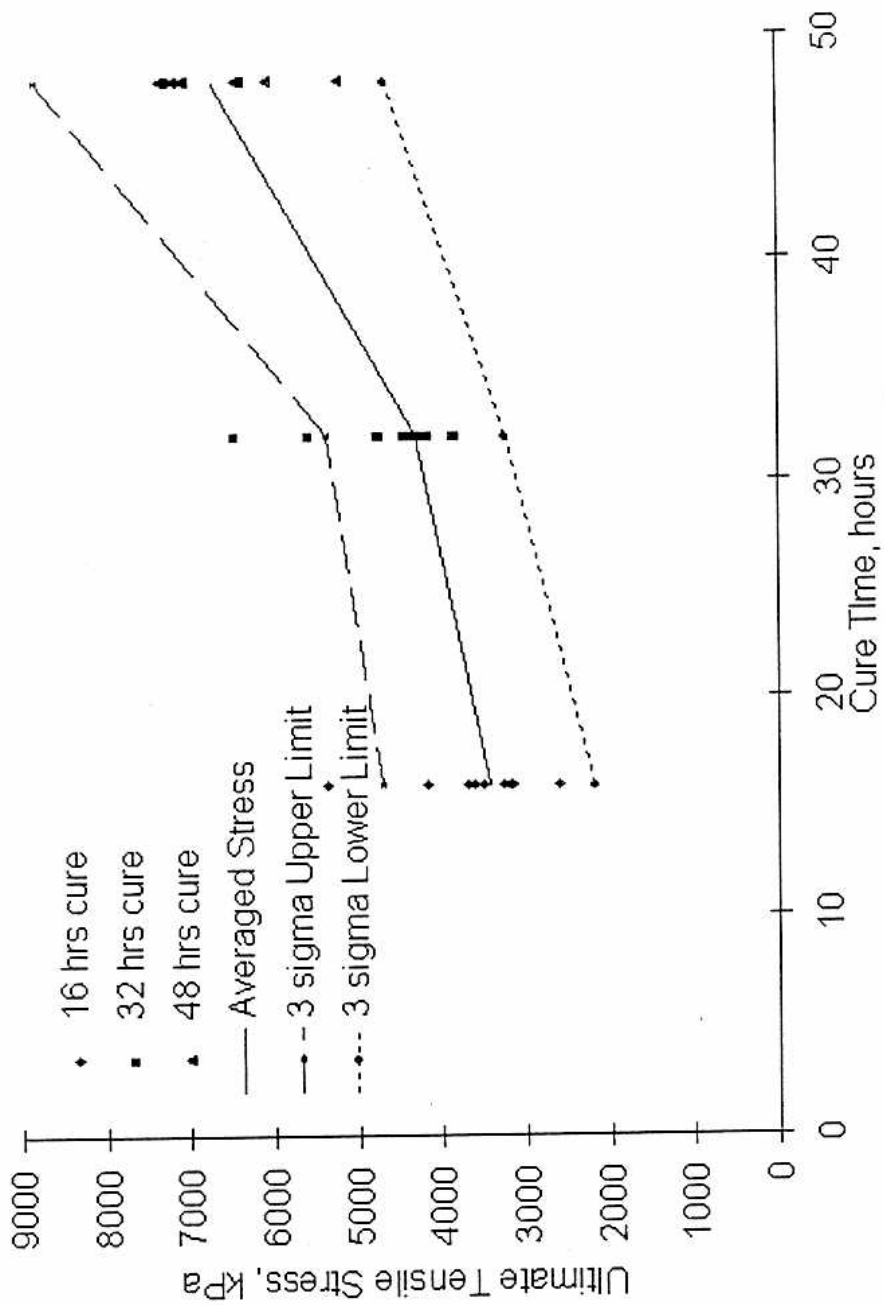


Figure 4.19: Ultimate Tensile Stress for Three Cure Times

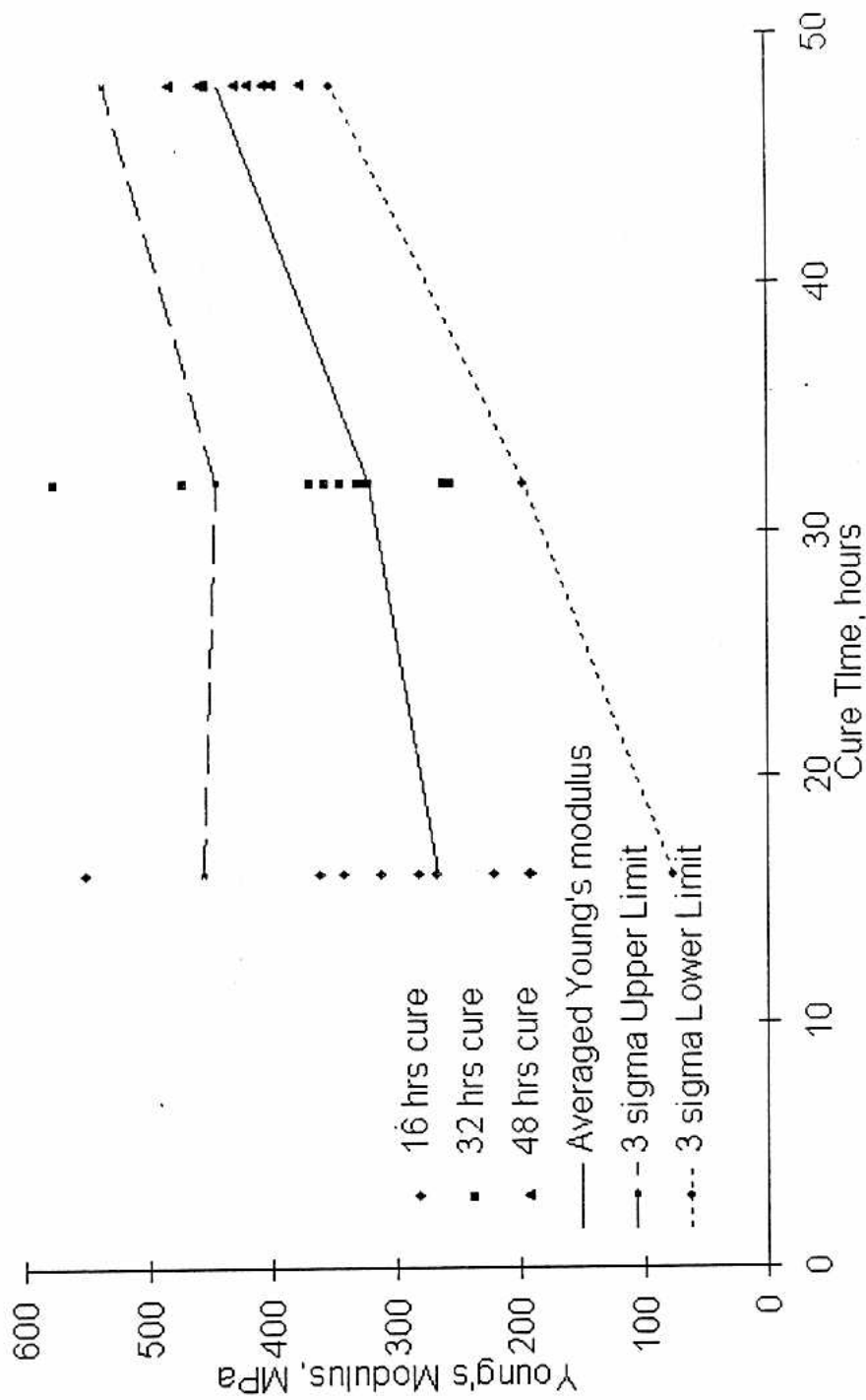


Figure 4.20: Modulus of Elasticity for Three Cure Times

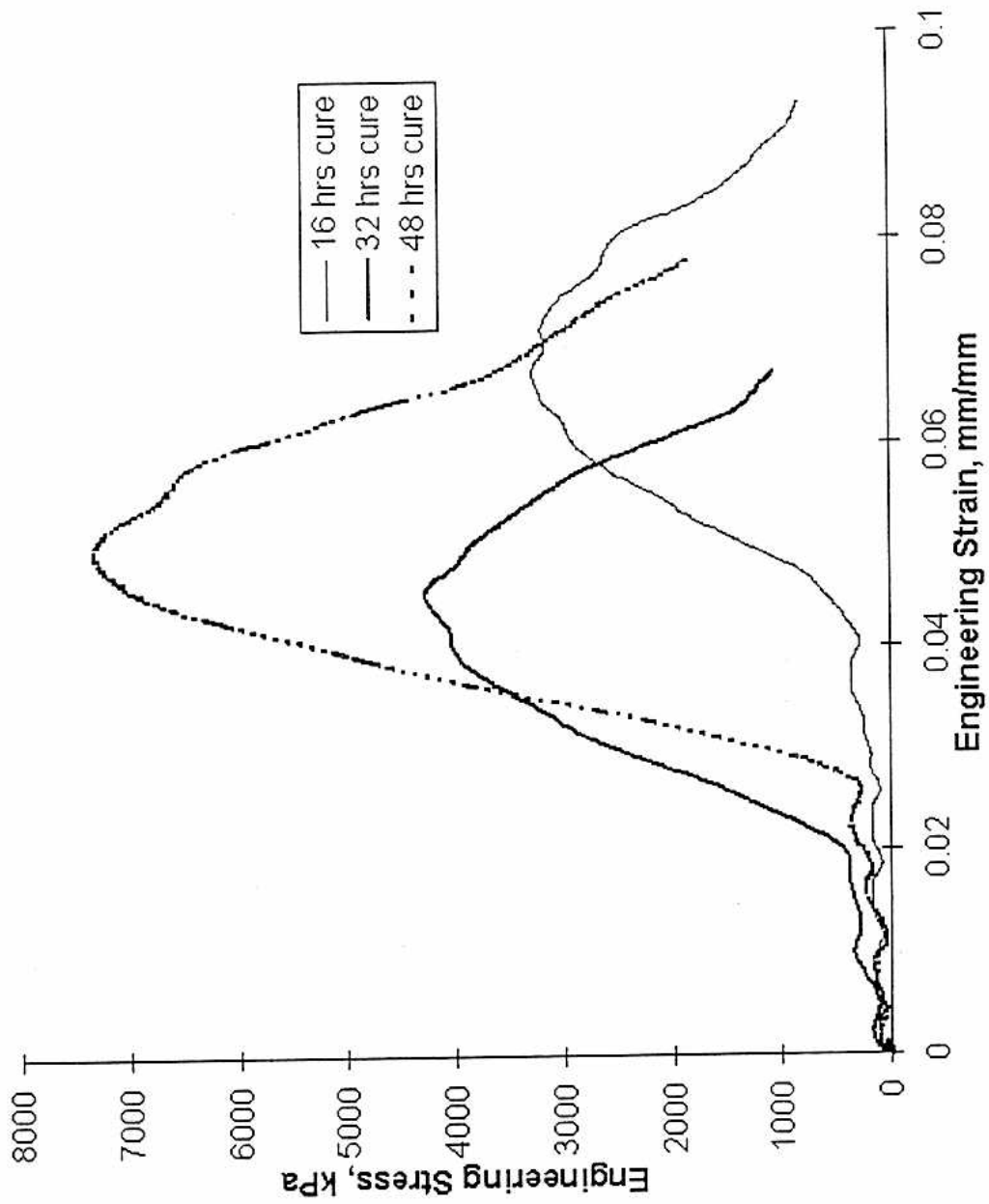


Figure 4.21: Tensile Stress-Strain Curves for the PVC Cement During the Cure Period

hours. Young's modulus increases 15 percent and 30 percent for the middle and last 16 hour portions of the cure cycle, respectively. The reader should ignore the backlash portions of the stress-strain curves because the backlash does not affect  $\sigma_{ult}$  or the modulus of elasticity.

**4.3.2.1.2 Shear Properties During the Cure Period** Figures 4.22 and 4.23 contain curves for the cure-time dependent increase in ultimate shear strength and modulus of rigidity, respectively. The shear strength had mean values of 3500, 4320, and 6580 kPa for the 16, 32, and 48 hour cure times, respectively. The modulus of rigidity had mean values of 108, 133, and 186 MPa for the 16, 32, and 48 hour cure times, respectively.

Figure 4.24 contains stress-strain curves for the shear samples tested at 16, 32, and 48 hours. As with the previous stress-strain curves presented, the curve contains three sections: backlash, elastic deformation, and plastic deformation.

This figure provides evidence that the adhesive gains significant strength and rigidity during the last 16 hours of the cure cycle. For the 16 to 32 hour cure period,  $\sigma_{ult}$  increases 24 percent, while the modulus of rigidity increases 23 percent. Both  $\sigma_{ult}$  and the modulus of rigidity increase 52 percent from 32 to 48 hours of cure.

The shear stress-strain curves also have an interesting stair step during the elastic portion of the curve. The exact cause of the stair step is unknown, but two theories could explain the phenomena. The first explanation is a stick-slip condition between incompletely formed crystals within the adhesive. The second theory concerns fluid pockets in the adhesive.

An incompletely formed crystalline structure, otherwise known as lamellae, in the adhesive could be the source for the stair step phenomena. The cement, which is an epoxy, develops a crystalline structure as it cures. Each lamellae grows out from an initiation point. This initiation point is where a polymer chain starts to fold into an organized three-dimensional shape, as opposed to the spaghetti noodle the chain resembles in the liquid phase.

During curing, the chain, which makes up a lamellae, pulls into an ordered shape. Figure 4.25 is a representation of a growing lamellae. When looked at from a side perspective, the chain resembles the corrugation in a cardboard box. The folding

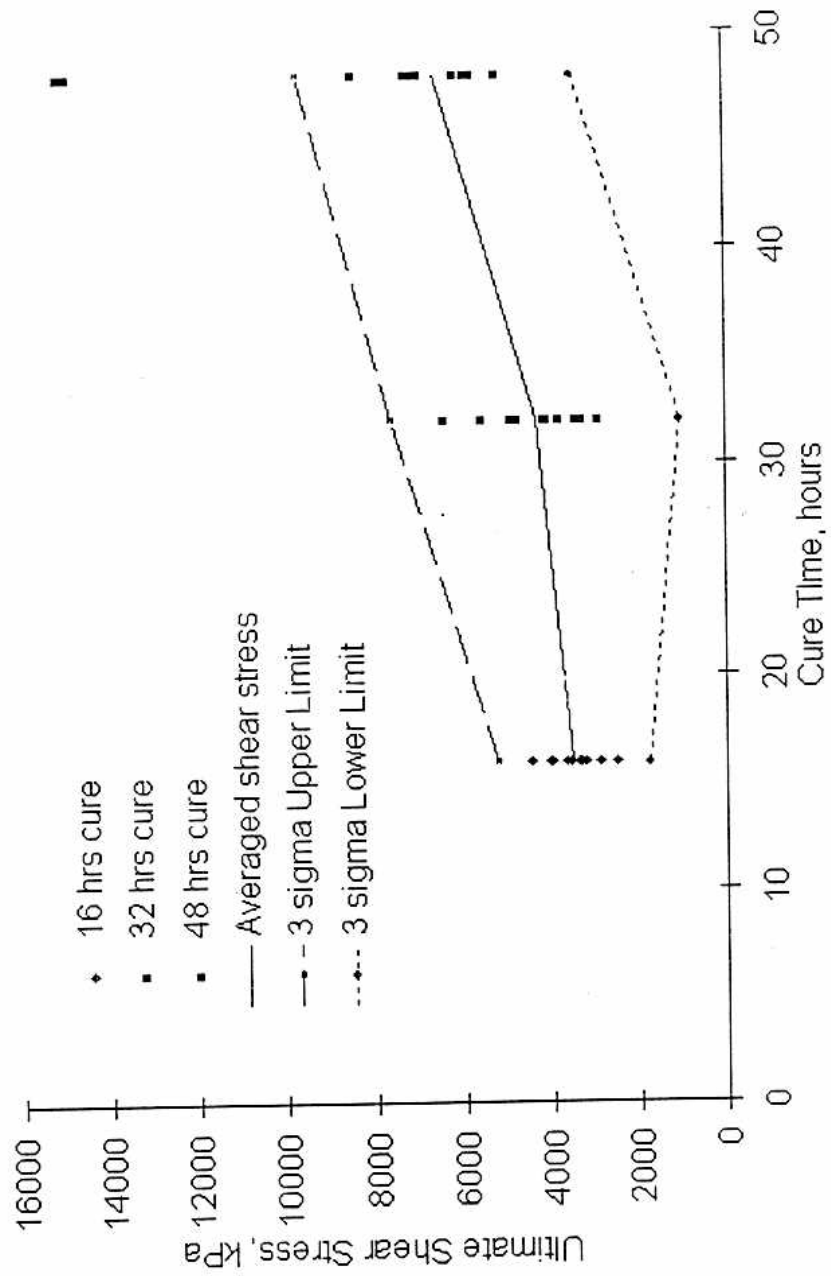


Figure 4.22: Ultimate Shear Stress for Three Cure Times

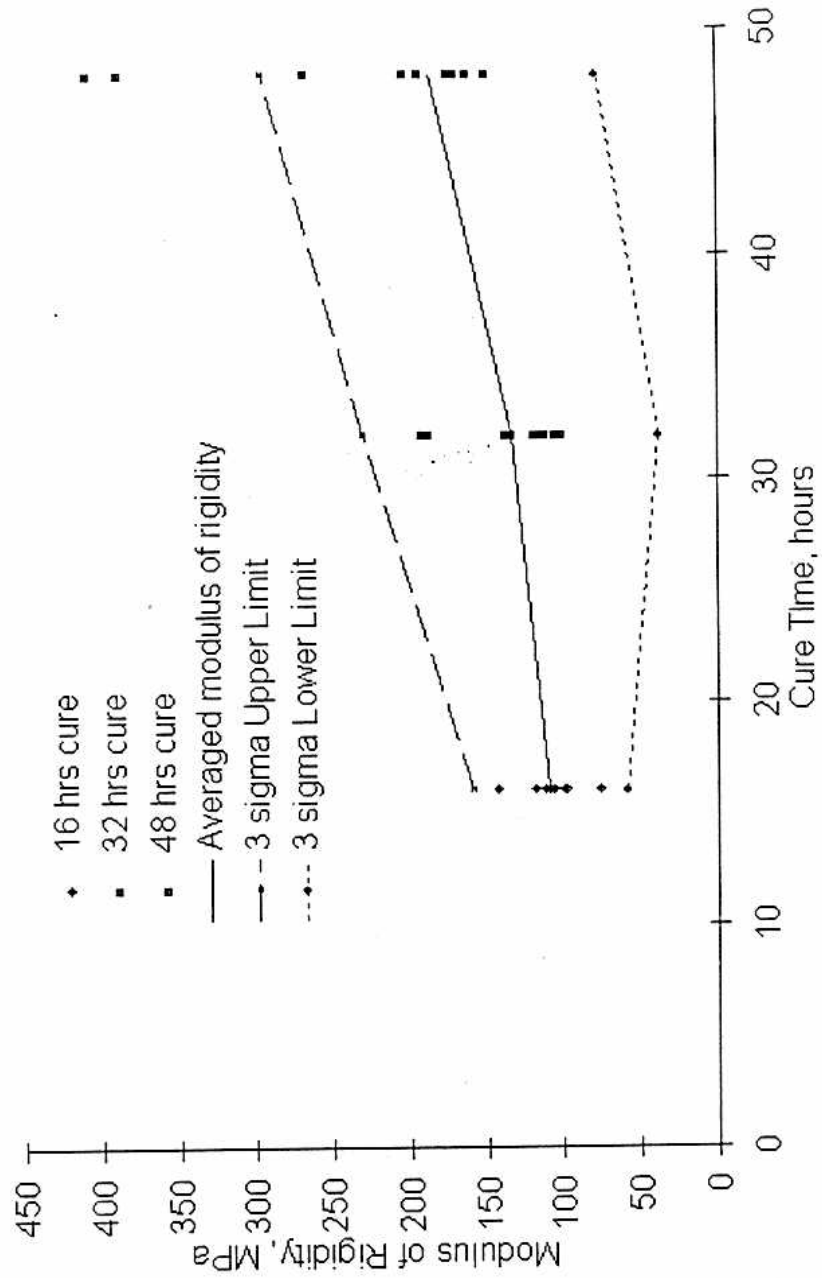


Figure 4.23: Modulus of Rigidity for Three Cure Times

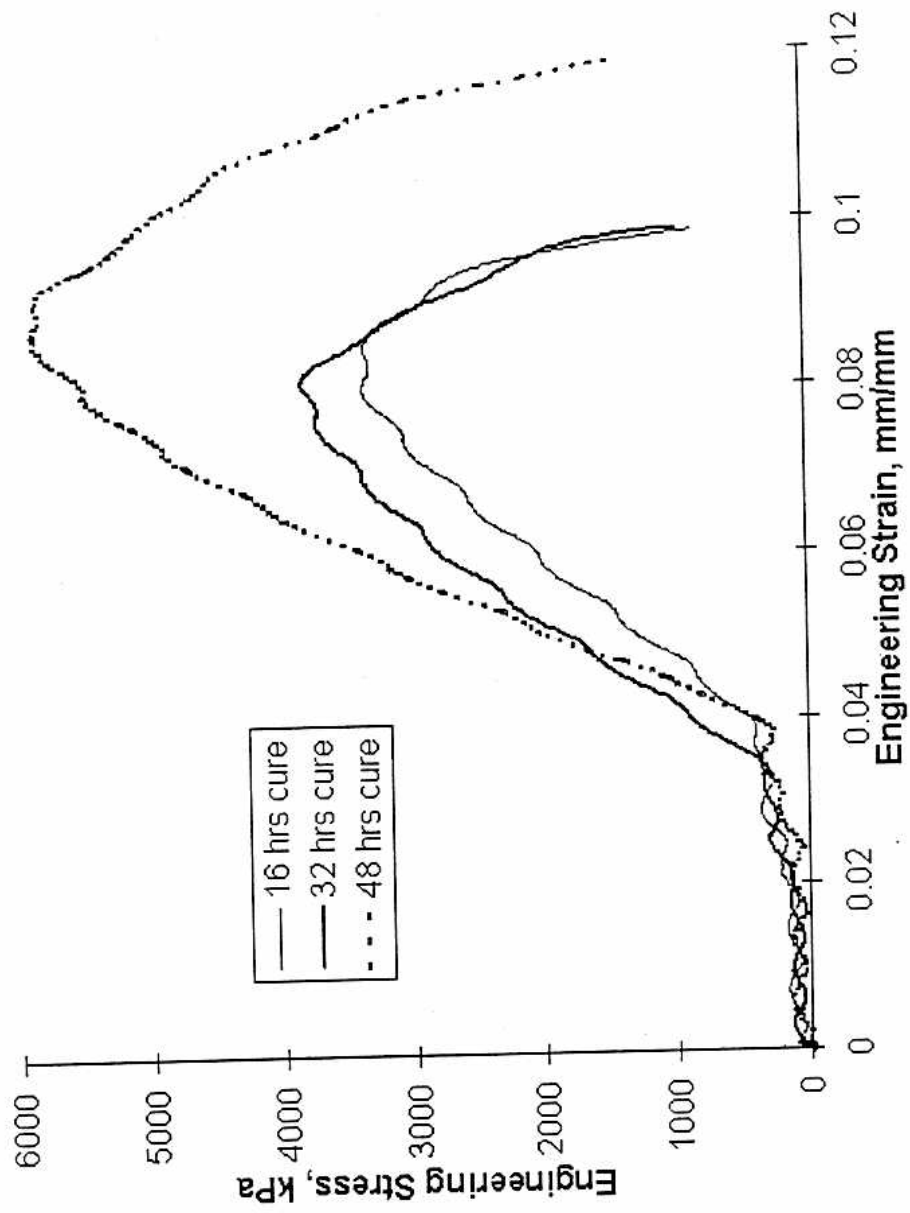


Figure 4.24: Shear Stress-Strain Curves for the PVC Cement During the Cure Period

tends to shape crystals into flat, pie-slice shapes.

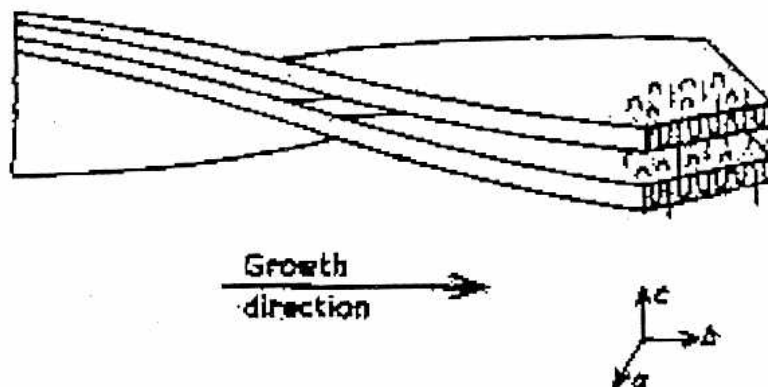


Figure 4.25: Schematic Representation of a Possible Model for Lamellae in Polyethylene Showing Polymer Folds and Intercrystalline Links (Young, 1991)

Inter and intra crystalline properties produce the strength of the polymer. The three-dimensional structure of the chain determines the intra crystalline strength of the polymer. The polymer side-chain groups also affect the three-dimensional shape of the chain. For PVC, the spine of the polymer is ethane molecules joined end-to-end, and the side chain is the chlorine.

The intercrystalline properties can influence strength also. As lamellae grow, the polymer chains are not perfectly ordered. Consequently, chains will coil into an adjacent lamellae. This cross-over tends to tie lamellae together, which increases strength and rigidity. Cross-links between chains and chain segments also increase strength. Vulcanized rubber, which has sulphur molecules as cross-links, is an example of a polymer that has cross-links to increase strength.

A more advanced discussion of this topic is beyond the scope of this thesis. Reference Young (1991) for a detailed discussion of polymer properties.

Liquid pockets could also be the source of the stair-step phenomena. As the partially-cured adhesive is stressed, the majority of the load is held by a matrix of lamellae. As the load is increased, the crystalline material becomes taught and eventually reaches a fracture point. After fracture, some of the load is transferred to the liquid, which is not stiff. If the load continues to be applied, the matrix will tend to rearrange in order to take up the load. Early in the cure cycle, the matrix is composed of many

loose crystals surrounded by liquid. Later in the cure cycle, the adhesive is mainly solid with a few liquid pockets.

This phenomena is analogous a piece of lace when stretched. As the lace is stretched the lace becomes taught and stiff. If a single strand of lace is cut, the lace matrix momentarily loses stiffness and stretches. The matrix will rearrange and become taught again if the load continues to be applied. This cycle can continue until all of the strands are cut. Referencing figure 4.24, the steep sections of the stairs happen as the matrix becomes taught. The lower angled portion of the stair occur when a portion of the matrix fails. This stair step phenomena also becomes less pronounced as the adhesive becomes more uniformly solid.

#### 4.3.2.2 Differences Between Control Groups

If the reader compares the control groups for the compatibility and cure period tests (the unexposed and fully-cured sample groups), an obvious difference between  $\sigma_{ult}$  and the moduli is apparent. The stress-strain curves for the tensile samples are also markedly different. Possible reasons for these differences are discussed here.

The strength and stiffness for both tensile-tested control groups are significantly different. The control group presented in Figure 4.13 has a mean ultimate strength of 14,000 kPa (2000 psi), while the control group presented in Figure 4.19 averaged 6000 kPa (500 psi). This change represents a 75 percent reduction in ultimate strength. The modulus of elasticity for both groups differ by 60 percent.

A dramatic difference between the yield characteristics of the two groups is also apparent if the reader references Figures 4.17 and 4.21. The test shown in Figure 4.17 exhibits little if any yielding. The control group presented in Figure 4.21 has a noticeable yield point.

Three different theories explain the difference in material properties between control groups. Differences in relative humidity is one explanation and the most likely cause of the difference. Age hardening and lot-to-lot differences between cements are the two other possible explanations.

The two control groups were prepared and tested in different seasons. The group presented in Figure 4.17 was tested in December, while the material presented in Figure 4.21 was tested in May. The atmospheric moisture content during these two

seasons is quite different in Minnesota. Since the moisture level in the air was higher for the second test, the water content in the second control group must have also been higher. Polymers are sensitive to water content, where extra moisture will weaken and soften a polymer.

Age hardening might have affected the material properties slightly. The first control group was stored for a month while the other samples were exposed to scintillator. The second control group only cured for 48 hours. During the extra storage time, the first group might have hardened somewhat.

The final and least likely explanation concerns lot-to-lot differences in the cement. Since the two control groups were tested more than six months apart, which happens to be the usable shelf life of the product, a new batch of adhesive was purchased. A possibility exists that the manufacturer failed to maintain a certain quality for the second batch, and consequently the strength is lower. This explanation is doubtful, as a 40 to 50 percent reduction in quality is highly unlikely.

#### 4.4 Flammability Testing

Since the detector is located in a mine, it is important that the design reduce any possibility of fire. A flammability test performed on the PVC and scintillator attempted to determine the sensitivity of these materials to heat and flame. First, a pan of scintillator was exposed to a heat source. Next, a propane torch was placed on a piece of PVC. Finally, a test module filled with scintillator was exposed to a flame. Bicron 517L was the scintillator used in all tests.

The first test determined the flammability of the scintillator. A cake pan was filled to a depth of approximately 0.32 cm (0.125 in) with scintillator. Then, the liquid was exposed to a torch for varying lengths of time. After 10 seconds, the liquid caught fire but self extinguished. After 20 seconds of exposure, the scintillator ignited and continued to burn until extinguished by the test personnel. The oil burned slowly and produced a yellow flame. The flash point for Bicron 517L is 102 degrees Celsius.

The second test evaluated the flammability of PVC. A strip of PVC, held in a vice, was exposed to a propane torch. The PVC burned during exposure, but self extinguished within 5 seconds after the flame was pulled away.

For the final test, a short test module was exposed to a propane torch. The module was approximately 30.5 cm (12 in) long, and one end was open to the atmosphere. The module was filled with scintillator to approximately an 8 inch depth. The flame was placed approximately 2.5 cm (2 in) below the fill level.

On the first side tested, the exposure time was 1.5 minutes in 15 second intervals. In this time, small seep holes developed in the side of the extrusion. The scintillator that leaked out ignited. After removing the torch, the module burned for 20 seconds, and then the flame extinguished.

The other side of the module was also exposed. After 45 seconds of steady flame contact, scintillator started to leak and then ignited. The torch was pulled away, and the burning scintillator self extinguished. The module was again exposed to the flame for another 20 seconds, and the module again started to burn. This time the fire burned for 2 to 3 minutes.

The fire originally was on the outside of the module, but then moved to the inside. Scintillator leaking out of the extrusion fed the fire on the outside. Fire streaks developed as the scintillator caught fire and then dripped into a pan below the extrusion. The PVC charred and blackened but never burned. When the fluid level reached the seep holes, the fire moved to the inside of one of the channels. The internal flame weakened and died as the oxygen inside the tubes was consumed by combustion.

The PVC produced an extinguishing effect on the fire. The burning scintillator is not hot enough to ignite the PVC, but it is hot enough to keep the PVC molten. The author speculates that when small seep holes develop the molten PVC flows into the holes and kills the flame, as in the first case. If larger holes develop, either the scintillator produces a cooling effect on the PVC to keep the leaks open, or the PVC can not flow far enough to close the leak.

# Chapter 5

## Conclusion

This chapter discusses the results and conclusions of this thesis. Section 5.1 is a short review of this document. Section 5.2 presents the major conclusions of this work. Section 5.3 discusses what further work needs to be done to optimize this design and design process.

### 5.1 Review

This thesis furthers the work originally described by Berg (1997) on the liquid scintillator detector proposed for the MINOS experiment. In Berg's thesis, a design concept was presented, as well as the results of some preliminary structural integrity tests. This document describes the detailed design of the detector.

Chapter 2 discusses the design plan for the detector. Drawings are included of all components. The function of all major parts is also described.

Chapter 3 presents the manufacturing plan. The entire manufacturing process is detailed by flowcharts. This chapter also includes a description of the quality assurance program.

Chapter 4 describes the tests performed to determine structural integrity. Prototype modules were tested for dimensional stability. The seals were tested for robustness. The PVC cement was also tested for compatibility with the liquid scintillator.

## 5.2 Conclusions

This thesis describes the complete design of liquid scintillator, high-energy particle detector. All major components of the active detector have been designed on Pro/Engineer with full-scale computer models of all parts. The designs not only provide the functionality required but have also been optimized to facilitate manufacturing. For example, the endcap has a near constant wall thickness and drafted sides, both of which are required for injection molded parts:

A complete manufacturing and quality control plan was developed for the liquid scintillator design utilizing PVC extrusions as module cases. The manufacturing plan presented a process for control of material flow on the manufacturing floor. The quality control plan describes a comprehensive process for ensuring the performance of the active detector.

The PVC extrusions should perform adequately over the length of the experiment. Many extrusions were monitored for creep at elevated temperatures and pressures for 3000 hours. No significant evidence for creep was found.

The seal designs for both the endcap and bypass are acceptable. Several tests were performed on the seals to check their robustness. The seal designs are resistant to impact and other loads probable during handling, such as thermal cycling.

The PVC cement specified is compatible with liquid scintillator, Bicorn 517L. A battery of tensile and shear tests were performed on small PVC strips that had been bonded together using the cement. One test exposed the cement to scintillator. Evidence for bond strength degradation was not found.

## 5.3 Recommendations for Further Work

A number of items relating to the active detector design and manufacturing plans can be improved. This design only allows the fibers to be read from the top of the scintillator modules. A double-ended readout scheme has some advantages. The manufacturing plan, while comprehensive, can be optimized. The experiment also provides many opportunities to study how individual institutions within the collaboration interact.

The design presented in this thesis is for a single-ended readout. Single-ended readout

means that the fibers transmit the signal out of only one end of the module, in this case the top. Single-ended readout requires a mirror on the far end of the fiber. As mentioned previously, the current mirroring process only produces a mirror with 70% efficiency. Double-ended readout has the fiber extending from both ends of the module, so the light signals are monitored at either end of the module. This arrangement eliminates the mirror, and consequently increases the available light for data collection. Double-ended readout increases the sensitivity of the detector to low energy neutrino events.

The design presented does not address the issue of part tolerances. Over the width of a detector plane, considerable tolerance stack-up can develop. While the liquid detector design is somewhat forgiving for dimensional changes, this issue should be explored further.

Prototyping a small scale active detector plane will provide significant data to improve the assembly process. The manufacturing plan is mainly based on quality requirements developed by the collaboration, as well as requirements demanded by the design. Some of the plan was also developed as result of the small, yet incomplete, prototypes built during the research associated with this thesis. A pilot build will ultimately be more beneficial. The assembly and quality control machines also need to be designed and prototyped.

An area providing for a large volume of original research is a study of collaborations and their internal interactions during the design process. A short literature search on the study of large non-profit design groups did not produce any studies which have researched the behavior of these groups. A study to improve efficiency of collaborations, such as MINOS, would greatly benefit the high-energy physics community.

Modern high-energy physics experiments increasingly require enormous resource commitments. The MINOS collaboration contains more than 80 collaborators, and the experiment will most likely cost in excess of \$100 million. Since the government has reduced the budget for physics research while the demand for funding is increasing, improving efficiency for experiments like MINOS is important. Several areas of the process can be studied.

The MINOS collaborators are spread across three continents: North America, Europe, and Asia. Consequently, communication is a major concern. The collaboration

holds bi-monthly collaboration meetings, but attendance can be limited due to the travel distance required for some members. Therefore, localized groups within the collaboration can easily lose sight of the "big picture" because of their isolation, even though electronic mail is utilized as a communication medium. How is it possible to improve communication and understanding between groups?

Different sub groups within the collaboration can also duplicate efforts because of their isolation. Under some circumstances, this duplication can be beneficial. For example, when examining experimental data, obtaining reviews from several different groups can be beneficial. Persons of different backgrounds may draw different yet significant findings from the same data set. More commonly, duplication causes inefficiency, as in the case of two separate groups designing the same machine while not coordinating their progress. What duplication is good or bad, and how can the project manager tell the difference between the two types? Could using a comprehensive on-line design site help? Is there an optimum personality type to manage organizations like MINOS?

Collaborations of this type also tend to be highly political. How can this political nature be managed?

The research presented in this thesis represents a complete conceptual design and manufacturing plan for a liquid scintillator active detector. As discussed earlier, some optimization remains to be done in the design. However, the design discussed in this thesis is expected to perform safely throughout the service life of the detector.

# References

- Abbes, M., 1996, "The Bugey 3 Neutrino Detector", Nuclear Instruments and Methods in Physics Research A, vol. A374, pp. 164-187.
- Aglietta, P. et al., 1995, "The LVD experiment at Gran Sasso", Il Nuovo Cimento, vol. 18C, no. 6, pp. 629-645.
- Allison, W. W. M. et al., 1996, "The Soudan 2 detector. The Design and Construction of the Tracking Calorimeter Modules", Nuclear Instruments and Methods in Physics Research A, vol. A376, pp. 36-48.
- Athanassopoulos, A. et al., 1997, "The liquid scintillator neutrino detector and LAMPF neutrino source", Nuclear Instruments and Methods in Physics Research A, vol. 388, pp. 149-172.
- Ayres, D. S., 1998, "Detectors for the MINOS Long-Baseline Neutrino Oscillation Experiment", Nuclear Physics B (Proceedings Supplements), vol. 61B, pp. 12-20.
- Barnett, R. M., et al, 1996, "Review of Particle Physics", Physical Review D (Particles and Fields), vol. 54, no. 1, pt. 1, pp. 85-89.
- Berg, T. 1998, "Structural Design of a High Energy Particle Detector Using Liquid Scintillator", Master's Thesis, University of Minnesota.
- Brandrup, J. and E. H. Immergut, ed., 1989, "Polymer Handbook", Wiley, New York, New York, 3rd edition.
- Brown, C. et al., 1989, "D0 Muon System with Proportional Drift Tube Chambers", Nuclear Instruments and Methods in Physics Research A, vol. A279, pp. 331-338.
- Fermilab, 1998a, "Loners of the Universe", Information Brochure, Fermi National

- Accelerator Laboratory, Batavia, Illinois.
- Fermilab, 1998b, "Neutrino Physics", Information Brochure, Fermi National Accelerator Laboratory, Batavia, Illinois.
- Ferry, J. D., 1980, "Viscoelastic Properties of Polymers", Wiley, New York, New York, 3rd edition.
- Fitch, J., et al., 1984, "A Novel Proportional Drift Tube System", Nuclear Instruments and Methods in Physics Research, vol. 226, pp. 373 - 375.
- Gallagher, H. M., 1996, "Neutrino Oscillation Searches with the Soudan 2 Detector", Ph.D. Thesis, University of Minnesota, Minneapolis, MN.
- Goodman, Maury, Spring, 1998, "Searching for Neutrino Oscillations", Beamline, pp. 9-16.
- Grayer, G. H., 1996, "Possible Use of RPCs in the MINOS Experiment", Sci Acta Quad Dottorato, vol. 11, no. 1, pp. 279-284.
- Kearns, E., 1994, "Upward-Going Muon Physics with the MACRO Detector", American Institute of Physics Conference Proceedings: Intersections Between Particle and Nuclear Physics, vol. 338, pp.874-879.
- Pontecorvo, B., 1982, "The Infancy and Youth of Neutrino Physic", Journal de Physique Colloque, vol. 43, C-8, pp.C8/221-236.
- Reines, Frederick, 1982, "Nue Interactions at Fission Reactors - Past and Future", Proceedings of the 8th International Workshop on Weak Interactions and Neutrinos, September, 6-11, 1982, Spain, pp. 6-11.
- Roark, R. J. and Young, W. C., 1975, "Fourmulas for Stress and Strain", 5th edition, McGraw-Hill, New York, New York, pp. 188-189.
- Super Kamiokande Collaboration, 1998, World Wide Web, <http://neutrino.phys.washington.edu/superk/>.
- Wojcicki, Stanley, May, 15, 1998, "Good  $\nu$ 's", FermiNews, pp.10-15.
- Young, R. J. and P. A. Lovell, 1991, "Introduction to Polymers", Chapman & Hall, London, UK, 2nd edition.

# Appendix A

## Glossary of Terms

This thesis discusses a topic that may be unfamiliar to many engineers. To assist the reader in understanding the subject matter, a list of terms used in this text is presented.

**Active Detector** The part of the MINOS detector that detects an event. The active detector design is discussed in this thesis. See also, passive detector.

**Bypass** A part that routes the fiber optic strands around the magnet hole.

**Event** The interaction of a neutrino with matter.

**MINOS** Main Injector Neutrino Oscillation Search.

**Module** A grouping of channels. In this design, a module is a single PVC extrusion. See also, super module.

**Neutrino** A subatomic particle that is classified as a lepton. Neutrinos are so small that they can pass through solid matter.

**Passive Detector** The dense mass that increases the chance that an event will occur. The passive detector for this design is the sheets of steel. See also, active detector.

**Photodetector** Electronic hardware that detects an incoming photon and converts the light energy into electrical energy.

**Scintillator** The medium that converts radioactive energy into light energy. Two main scintillator options exist: liquid and solid. The liquid scintillator discussed in this text is mineral oil with psuedocumene. A typical solid scintillator is polystyrene doped with fluors.

**Super Module** A grouping of active detector and passive detector planes. As of September, 1997, a super module was 20 meters long and contained over 300 each of the active and passive detector planes. See also, module.

# Appendix B

## Deflection Predictions

This appendix contains deflection calculations for the creep testing discussed in section 4.1. The appendix is divided into three sections with each containing a separate calculation. The first section calculates the web deflection. The second section calculates the gap deflection using simply-supported end conditions. The third section calculates the deflection of the gap using double fixed-end conditions. Figure B.1 is a drawing of the forces and geometry used in the following calculations.

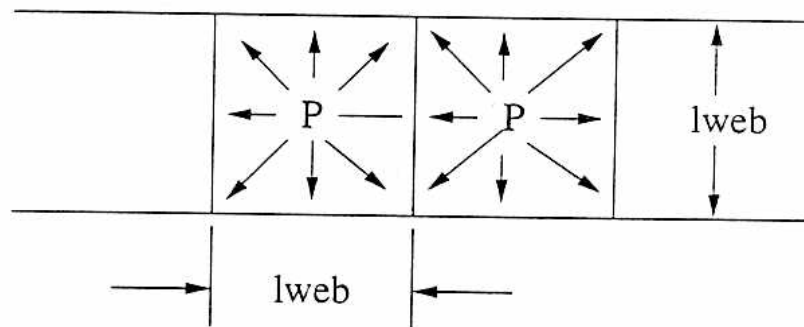


Figure B.1: Drawing of the Forces Exerted on a Test Module During Creep Testing

### B.1 Web Deflection

Assumptions:

1. Linear Elastic Deformation
2. Static Loading

3. No glass added to the PVC
4. Young's Modulus varies linearly between 40°C and 50°C.
5. Creep is negligible.
6. The cell is removed from outer wall interactions.
7. Fluid effects in the internal gas are negligible.

Known:

1. Wall thickness,  $t = 1.5$  mm
2. Internal Pressure,  $P = 144.8$  kPa (21 psi)
3. Length of web,  $l_{web} = 2$  cm
4. Width of a cell,  $w_{cell} = 2$  cm
5. Young's Modulus,  $E$   
 = 2964 MPa at 20°C  
 = 2930 MPa at 40°C  
 = 2427 MPa at 50°C from Brandrup (1989).

Calculating the pertinent areas and force:

$$f = Pw_{cell} = 2896 \text{ Nm}^{-1}$$

Calculating the deflection:

$$\delta_{web} = \frac{fl_{web}}{Et}$$

$$\text{At } 20^\circ\text{C: } \delta_{web} = 1.3(10^{-5}) \text{ m}$$

$$\text{At } 45^\circ\text{C: } \delta_{web} = 1.44(10^{-5}) \text{ m}$$

## B.2 Simply-supported Gap

Assumptions:

1. Linear Elastic Deformation
2. Static Loading
3. No glass added to the PVC
4. Young's Modulus varies linearly between 40°C and 50°C.
5. Creep is negligible.
6. The cell is removed from outer wall interactions.

7. Fluid effects in the internal gas are negligible.

Known:

1. Wall thickness,  $t = 1.5$  mm
2. Internal Pressure,  $P = 144.8$  kPa (21 psi)
3. Width of a cell,  $w_{cell} = 2$  cm
4. Poisson's ratio,  $\nu = 0.3$
5. Distributed load across the gap,  $q = 144.8$  kPa
6. Young's Modulus,  $E$   
= 2964 MPa at 20°C  
= 2930 MPa at 40°C  
= 2427 MPa at 50°C from Brandrup (1989).

Note: The actual measured deflection at the mid-span of the gap is the sum of the gap and web deflections.

Wide beam model: considering a beam of unit depth:

$$I = \frac{t^3}{12} = 2.81(10^{-12}) \text{ m}^3$$

From Roark:

$$\delta_{maxgap} = \frac{5Pl_{web}^4(1-\nu^2)}{384EI}$$

$$\text{At } 20^\circ\text{C: } \delta_{maxgap} = 0.00033 \text{ m}$$

$$\text{At } 45^\circ\text{C: } \delta_{maxgap} = 0.00037 \text{ m}$$

Total deflection for wide beam assumption:

$$\delta_{total} = \delta_{web} + 2\delta_{maxgap}$$

$$\text{At } 20^\circ\text{C: } \delta_{total} = 0.00034 \text{ m}$$

$$\text{At } 45^\circ\text{C: } \delta_{total} = 0.00038 \text{ m}$$

Narrow beam model:

$$\delta_{maxgap} = \frac{5Pl_{web}^4}{384EI}$$

$$\text{At } 20^\circ\text{C: } \delta_{maxgap} = 3.62(10^{-4}) \text{ m}$$

*In this context?*  
*2 (I?)*  
*5.5*  
*total*  
*Savelimsky @*  
*u.davis.edu*

$$\text{At } 45^{\circ}\text{C: } \delta_{maxgap} = 4.08(10^{-4}) \text{ m}$$

$$\text{At } 20^{\circ}\text{C: } \delta_{total} = 0.00038 \text{ m}$$

$$\text{At } 45^{\circ}\text{C: } \delta_{total} = 0.00042 \text{ m}$$

### B.3 Double Fixed-end Gap

Assumptions:

1. Linear Elastic Deformation
2. Static Loading
3. No glass added to the PVC
4. Young's Modulus varies linearly between  $40^{\circ}\text{C}$  and  $50^{\circ}\text{C}$ .
5. Creep is negligible.
6. The cell is removed from outer wall interactions.
7. Fluid effects in the internal gas are negligible.
8. Narrow beam

Known:

1. Wall thickness,  $t = 1.5 \text{ mm}$
2. Internal Pressure,  $P = 144.8 \text{ kPa}$  (21 psi)
3. Length of web,  $l_{web} = 2 \text{ cm}$
4. Young's Modulus,  $E$   
 $= 2964$  at  $20^{\circ}\text{C}$   
 $= 2930$  at  $40^{\circ}\text{C}$   
 $= 2427$  at  $50^{\circ}\text{C}$  from Brandrup (1989).

Note: The actual measured deflection at the mid-span of the gap is the sum of the gap and web deflections.

Considering a beam of unit depth:

$$I = \frac{t^3}{12} = 2.81(10^{-12}) \text{ m}^3$$

$$\delta_{maxgap} = \frac{Fl_{web}^4}{384EI}$$

$$\text{At } 20^{\circ}\text{C: } \delta_{maxgap} = 7.24(10^{-5}) \text{ m}$$

At 45°C:  $\delta_{maxgap} = 8.01(10^{-5})$  m

Total deflection:

$$\delta_{total} = \delta_{web} + \delta_{maxgap}$$

At 20°C:  $\delta_{total} = 0.000085$  m

At 45°C:  $\delta_{total} = 0.000095$  m